Cell Reports

Article

Infection with Bacteroides Phage BV01 Alters the Host Transcriptome and Bile Acid Metabolism in a Common Human Gut Microbe

Graphical Abstract

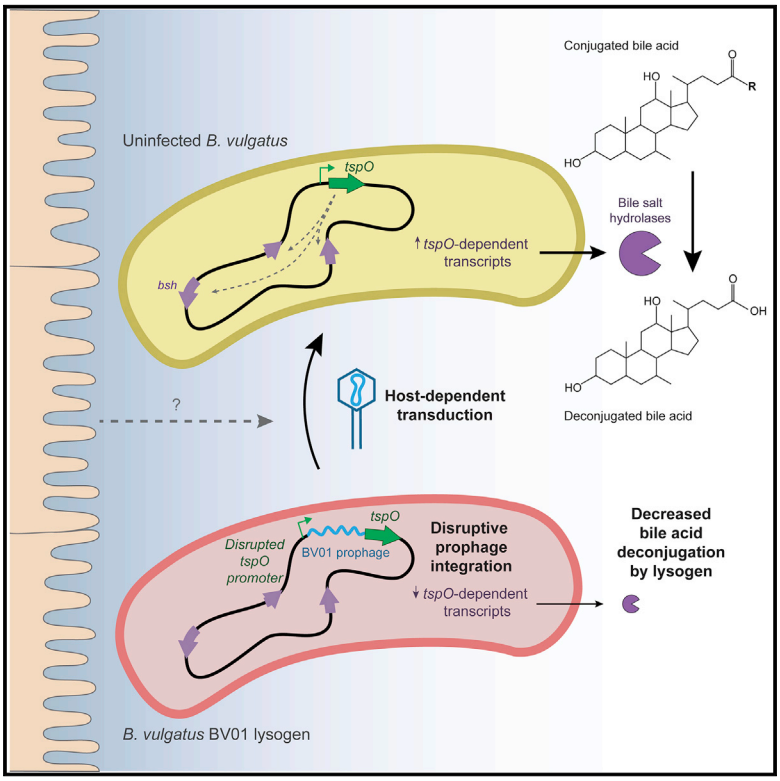

Highlights

- Integration of BV01 in the *tspO* promoter causes genome-wide transcriptome change
- *B. vulgatus* bile salt hydrolase (BSH) activity is repressed by BV01 integration
- Transduction of BV01 appears to be host dependent because it is only observed *in vivo*
- Phage BV01 is a member of the Salyersviridae phage family

Authors

Danielle E. Campbell, Lindsey K. Ly, Jason M. Ridlon, Ansel Hsiao, Rachel J. Whitaker, Patrick H. Degnan

Correspondence

patrick.degnan@ucr.edu

In Brief

Integrative phages can have myriad effects on bacterial hosts. Campbell et al. find that integration of Bacteroides phage BV01 into *Bacteroides vulgatus* disrupts expression of TspO, reducing bile acid deconjugation. This is predicted to affect gut colonization and interactions with the human host. BV01 belongs to the Salyersviridae family.

Campbell et al., 2020, Cell Reports *32*, 108142
September 15, 2020
https://doi.org/10.1016/j.celrep.2020.108142

CellPress

Cell Reports

CellPress
OPEN ACCESS

Article

Infection with Bacteroides Phage BV01 Alters the Host Transcriptome and Bile Acid Metabolism in a Common Human Gut Microbe

Danielle E. Campbell,[1] Lindsey K. Ly,[2,3] Jason M. Ridlon,[2,3,4] Ansel Hsiao,[5] Rachel J. Whitaker,[1,4] and Patrick H. Degnan[5,6,*]

[1]Department of Microbiology, University of Illinois, Urbana, IL 61801, USA
[2]Division of Nutritional Sciences, University of Illinois, Urbana, IL 61801, USA
[3]Department of Animal Sciences, University of Illinois, Urbana, IL 61801, USA
[4]Carl R. Woese Institute for Genomic Biology, University of Illinois, Urbana, IL 61801, USA
[5]Department of Microbiology and Plant Pathology, University of California, Riverside, Riverside, CA 92521, USA
[6]Lead Contact
*Correspondence: patrick.degnan@ucr.edu
https://doi.org/10.1016/j.celrep.2020.108142

SUMMARY

Gut-associated phages are hypothesized to alter the abundance and activity of their bacterial hosts, contributing to human health and disease. Although temperate phages constitute a significant fraction of the gut virome, the effects of lysogenic infection are underexplored. We report that the temperate phage, Bacteroides phage BV01, broadly alters its host's transcriptome, the prominent human gut symbiont *Bacteroides vulgatus*. This alteration occurs through phage-induced repression of a tryptophan-rich sensory protein (TspO) and represses bile acid deconjugation. Because microbially modified bile acids are important signals for the mammalian host, this is a mechanism by which a phage may influence mammalian phenotypes. Furthermore, BV01 and its relatives in the proposed phage family Salyersviridae are ubiquitous in human gut metagenomes, infecting a broad range of *Bacteroides* hosts. These results demonstrate the complexity of phage-bacteria-mammal relationships and emphasize a need to better understand the role of temperate phages in the gut microbiome.

INTRODUCTION

The human gut is colonized by a dense and diverse microbial community comprised of bacterial, archaeal, and fungal cells as well as the viruses that infect them. This gut microbiome is vital for human health and development and is linked to an increasingly long list of disease states (Hills et al., 2019; Schmidt et al., 2018). Recent work has specifically implicated the gut phageome in disease, including inflammatory bowel disease (Norman et al., 2015), malnutrition (Reyes et al., 2015), AIDS (Monaco et al., 2016), colorectal cancers (Hannigan et al., 2018), and hypertension (Han et al., 2018). Broadly, gut phages act as important modulators of bacterial community structure (Hannigan et al., 2018; Khan Mirzaei et al., 2020; Moreno-Gallego et al., 2019) and metabolism (Hsu et al., 2019). Despite their apparent importance, little is known about how most gut-associated phages interact with their bacterial hosts (Mirzaei and Maurice, 2017).

Bacteroides is one of the most common and abundant bacterial genera in the distal human gut. The genus is known to degrade a diversity of complex carbohydrates (El Kaoutari et al., 2013; Salyers et al., 1977) and interact with host immune cells (Hickey et al., 2015; Shen et al., 2012). In a single human host, many *Bacteroides* species and strains coexist, competing for nutrients under changing environmental conditions caused by host diet (Tuncil et al., 2017), host metabolites (Ridlon et al., 2016), host immune system activities (Cullen et al., 2015; Planer et al., 2016), and phage predation (Porter et al., 2020). Moreover, horizontal gene transfer plays an important role in shaping the evolution and function of *Bacteroides* genomes (Coyne et al., 2014; Lange et al., 2016). How the diversity of *Bacteroides* strains in the human gut persists over time in such a dense, dynamic, and competitive environment is likely to have many reasons and is perhaps afforded by their highly plastic genomes.

Phage diversity and phage-host interactions in most commensal gut-associated bacteria, including *Bacteroides* species, is underexplored, but bioinformatics predictions of *Bacteroides* phages have been made (Krupovic and Forterre, 2011; Lange et al., 2016). Currently, the most abundant gut-associated phages are crAssphages (Dutilh et al., 2014; Koonin and Yutin, 2020; Yutin et al., 2018), a group of related lytic phages that infect *Bacteroides intestinalis* and potentially other species. CrAssphages demonstrate how traditional phage techniques (e.g., agar overlay plaque assays) are not reliable for *Bacteroides* hosts (Shkoporov et al., 2018), likely because of heterogeneity in capsular polysaccharide composition in isogenic cultures

(Krinos et al., 2001; Patrick et al., 2010). In fact, deletion of all capsular polysaccharide synthesis loci allows isolation of many phages on the host *Bacteroides thetaiotaomicron* VPI-5482 (Porter et al., 2020). Most phages isolated against *Bacteroides* hosts so far exhibit an obligately lytic lifestyle (Jofre et al., 2014; Porter et al., 2020; Shkoporov et al., 2018; Tartera and Jofre, 1987) despite the potentially important role of lysogeny in phage-host interactions in the gut, where at least 17% of the gut phageome is predicted to be temperate (Minot et al., 2011; Ogilvie et al., 2013).

Prophage-host interactions have the potential to cause complex alterations to the host phenotype because of the temperate lifestyle having two distinct phases: lysogeny and lysis (Bondy-Denomy and Davidson, 2014; Howard-Varona et al., 2017). Unlike most strictly lytic phages, temperate phages more readily transfer beneficial genes between hosts, such as antibiotic resistance genes (Abeles et al., 2015) and auxiliary metabolic genes (Anantharaman et al., 2014; Sullivan et al., 2005). Some phage regulatory machinery expressed from prophages can modulate transcription of host genes, resulting in altered phenotypes (Berger et al., 2019; Hernandez-Doria and Sperandio, 2018). Integration of prophages into the host genome may also disrupt or enhance the activity of surrounding chromosomal genes (Carey et al., 2019; Chen et al., 2019; Feiner et al., 2015; Rabinovich et al., 2012). Although much is known about how these prophage-host interactions contribute to virulence in pathogens (Bensing et al., 2001; Jermyn and Boyd, 2002; Nakayama et al., 1999; Sekulovic and Fortier, 2015; Winter et al., 2010), very little is known about how phages modulate the activities of commensals.

Here we identified an active prophage, Bacteroides phage BV01, in a genetically tractable host strain, *B. vulgatus* ATCC 8482, and characterized its effects on the host's transcriptome and phenotype. Further, we determine that BV01 represents a larger group of *Bacteroides*-associated phages comprising the proposed virus family Salyersviridae that common in the human gut phageome. This work provides insight into how *Bacteroides* react to temperate phage infection and establishes a model system for exploring complex phage-host interactions in an important human symbiont.

RESULTS

Bacteroides Phage BV01 Is a Prophage in *B. vulgatus* ATCC 8482

Bacteroides phage BV01 was partially predicted previously with the computational tool ProPhinder in the genome of *B. vulgatus* ATCC 8482 and deposited in a CLAssification of Mobile genetic Elements (ACLAME) database (Leplae et al., 2010; Lima-Mendez et al., 2008). Through comparative genomics and re-annotation of the host genome, we extended the predicted BV01 prophage to 58.9 kb (NCBI RefSeq: NC_009614.1; 3,579,765–3,638,687), which comprises 75 predicted open reading frames (ORFs) (Table S1). This larger predicted region is consistent with an earlier report of a prophage induced from this bacterial strain colonizing gnotobiotic mice (Reyes et al., 2013). BV01 encodes genes suggesting a temperate lifestyle with a putative phage repressor and anti-repressor as well as a holin-lysin-spanin operon for lytic release of phage progeny (Table S1; Figure 1A; Kongari et al., 2018; Young, 2014).

BV01 is detectable outside of host cells in the supernatants of *in vitro* cultures as a DNase-protected, double-stranded DNA (dsDNA) genome by shotgun sequencing (Figure 1A). Assembly of sequencing reads from free BV01 phage DNA results in a circular contig that spans the phage attachment site (*attP*). BV01 *attP* is identical to the left and right attachment sites (*attL* and *attR*, respectively), a pair of 25-bp direct repeat sequences (5′-GTCTAGTTTAGTTTTTGTGTTGTAA-3′), suggesting that BV01 enters a circular intermediate before replication.

Routine detection of phage BV01 in DNase-treated, cell-free supernatants by PCR suggests that it is spontaneously induced. Furthermore, examination of the phage-to-host ratio by qPCR revealed that it remained approximately 1 throughout log and stationary phase host growth (Figure 1B), which is expected for phages that are spontaneously induced (Baugher et al., 2014; Bonanno et al., 2016). We have yet to identify *in vitro* induction conditions that increase phage BV01 production above this background level detectable by qPCR. Subinhibitory concentrations of the antibiotics norfloxacin, mitomycin C, tetracycline, and erythromycin; UV irradiation; or co-culture with gut-associated microbes do not increase BV01 production. Furthermore, attempts to visualize BV01 by transmission electron microscopy were not successful, likely because of the small number of phage particles produced.

An isogenic cured lysogen (ΔBV01) strain was constructed by allelic exchange with the corresponding chromosomal *attB* region of an uninfected *B. vulgatus* strain (Figure 1A). No apparent fitness effect of BV01 infection was detected *in vitro* because growth of the lysogen (wild-type [WT]) and cured lysogen strains (ΔBV01) are not significantly different (Figures 1C and 1D). This further supports the conclusion that spontaneous induction of BV01 occurs at a low rate and that sporadic cell lysis events do not have an effect on cell density.

Despite sequence evidence of BV01 phage particles in the culture supernatants, BV01-containing supernatants were never found to produce new infection. No lytic infection was detected using plaque assays (Kropinski et al., 2009) with 10 *B. vulgatus* isolates (Table S4), the *B. vulgatus* cured lysogen (ΔBV01), *B. thetaiotaomicron*, and 4 *B. dorei* isolates on four different growth media: tryptone-yeast extract-glucose broth (TYG), brain heart infusion (BHI) agar supplemented with 10% defibrinated horse blood (HB), BHI supplemented with hemin and menadione (BHI-HM) (Thornton et al., 2012), and supplemented TYG (TYG_S) (Goodman et al., 2009). Enrichment of infectious BV01 particles was attempted by passaging BV01-containing supernatants on *B. vulgatus* cured lysogen (ΔBV01) every day for 10 days (Shkoporov et al., 2018). However, enrichment was unsuccessful because subsequent plaque assays on naive cured lysogen did not yield any plaques. The same panel of 15 *Bacteroides* strains was tested for formation of lysogenic infection using non-concentrated or 200× concentrated BV01-containing supernatants. However, no novel infection was detected by PCR with primers designed to span the attachment site. To further test for new lysogenic infection, BV01 was tagged with a copy of *tetQ*, conferring tetracycline resistance, using allelic exchange. Five recipient strains, 4 *B. vulgatus* hosts and 1

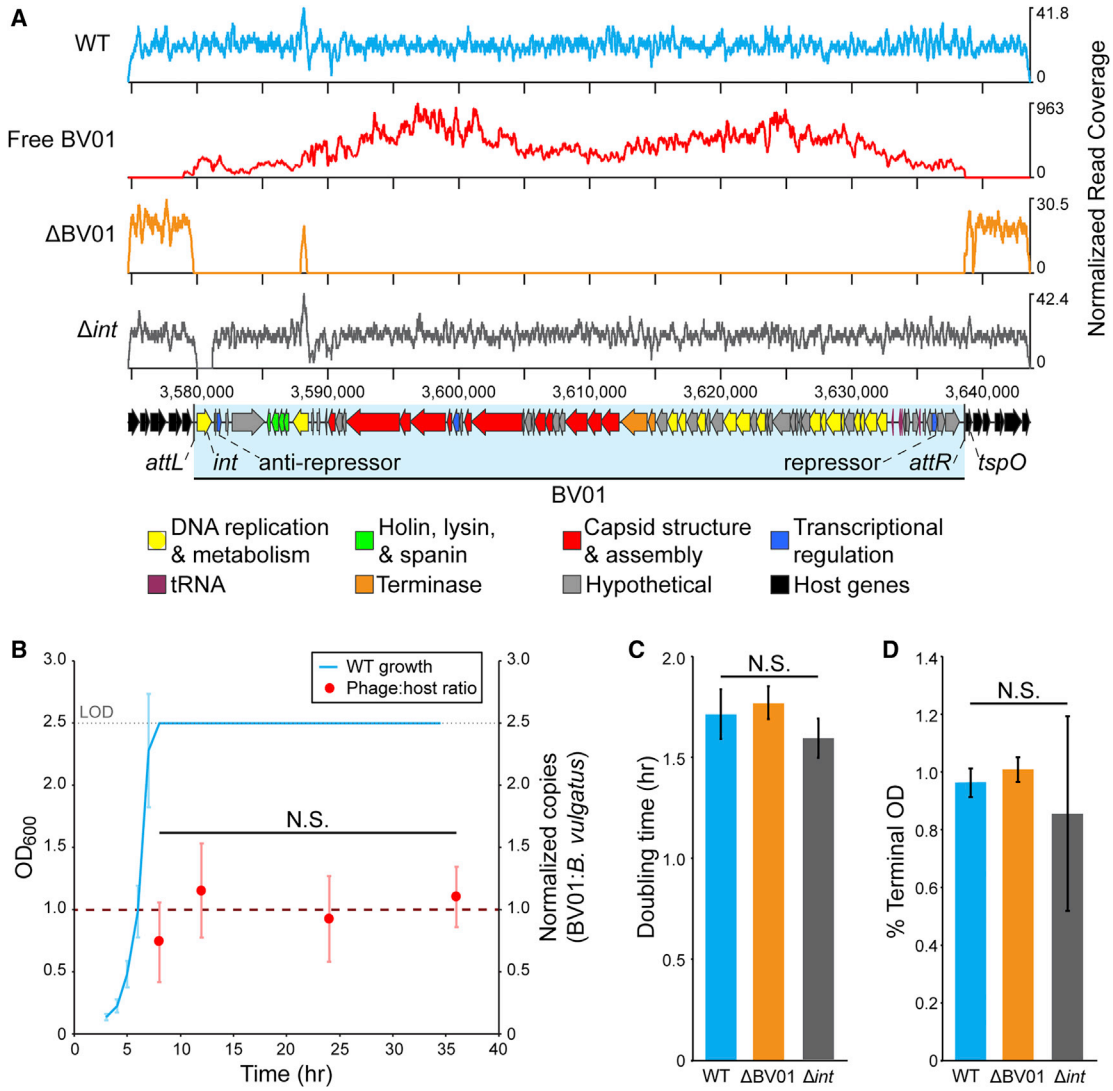

Figure 1. Phage BV01 Is Spontaneously Induced in Culture

(A) DNA sequencing reads mapped to the BV01 prophage region. Reads from sequencing of *B. vulgatus* genomic DNA (WT) or isolated phage DNA (free BV01) were normalized to the total number of reads after trimming and are represented as a coverage curve. A cured lysogen (ΔBV01) and integrase deletion mutant (Δ*int*) of *B. vulgatus* were confirmed by shotgun sequencing of genomic DNA (Tables S2 and S3). The coverage peak at position ~3,588,000 nt in ΔBV01 is attributed to a homologous sequence elsewhere in the *B. vulgatus* genome. Putative functional categories of BV01 genes are indicated by color; see Table S1 for full BV01 gene annotation.

(B) BV01 is produced at low levels at all stages of host growth. WT cultures were grown in triplicate for 36 h, and BV01 and host abundance were monitored by qPCR. By log phase, cultures reached the limit of detection (LOD) of the spectrophotometer.

(C and D) Lysogeny with phage BV01 does not affect (C) doubling time or (D) terminal optical density (OD) *in vitro*. Doubling times and terminal ODs were calculated for wild-type (WT), cured lysogen (ΔBV01), and integrase deletion (Δ*int*) strains and averaged across three replicates.

Statistical analyses were performed with one-way ANOVA. N.S., not significant. Phage:host ratio $df = 3$, $F = 4.03$, $p = 0.051$. Doubling time $df = 2$, $F = 2.55$, $p = 0.157$. Percent terminal OD $df = 2$, $F = 6.59$, $p = 0.101$. All error bars represent standard deviation.

B. dorei host, were tagged with erythromycin resistance with pNBU2-*bla*-*ermG* (Table S4). Double antibiotic selection found no new lysogens after attempted infection assays using BV01-*tetQ* supernatants or 200× concentrated BV01-*tetQ* supernatants or after 24-h co-culture of donor and recipient strains. We conclude that BV01 is a latent prophage *in vitro*, which is further supported by transcriptional data showing that BV01 exists in a largely repressed state (Figure S1A), a state likely maintained by the predicted phage repressor (BVU_RS14475), the most highly transcribed gene in the BV01 prophage (Figure S1A).

The only infectious conditions that were identified for BV01 are in a gnotobiotic mouse model (Figure 2A). Within 1 day of gavage, BV01-*tetQ* transductants were identified on doubly selective medium from mouse pellets from 4 of the 7 mice. Over the course of the 11-day experiment, transductants were

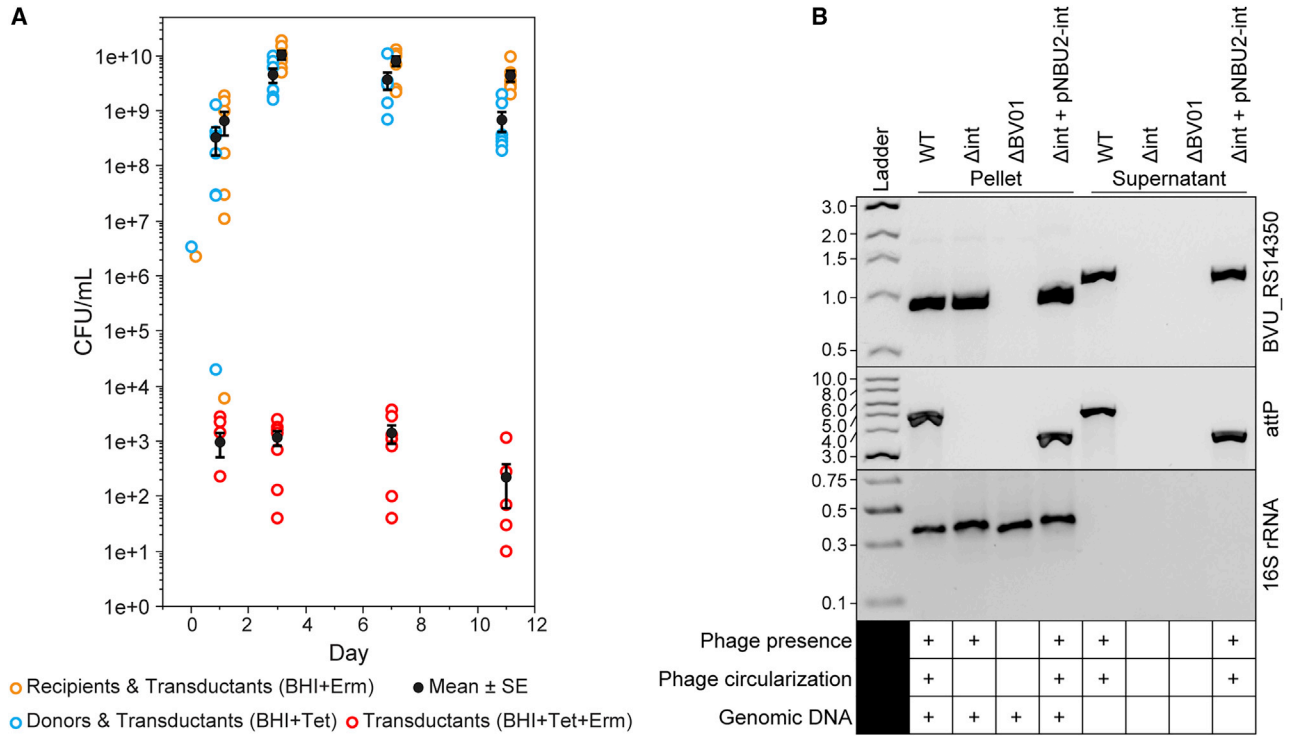

Figure 2. Transduction, Excision, and Circularization of Phage BV01

(A) BV01 can transduce uninfected hosts in gnotobiotic mice (n = 7). Mice were gavaged with an equal mixture of BV01-*tetQ* lysogen and erythromycin-tagged cured lysogen (day 0). Recipient, donor, and transductant cells were identified by plating on medium with erythromycin (Erm) or tetracycline (Tet). Calculated means and standard errors (SE) are shown in black.

(B) Excision and circularization activities of the BV01 integrase are confirmed by PCR from late stationary phase cultures of four strains: WT, Δ*int*, ΔBV01, and the *int* complement strain using a pNBU2 integrative plasmid (Δ*int* + pNBU2-*int*). The presence of phage DNA was detected by amplification of a phage marker gene (BVU_RS14350). Amplification across the phage attachment site (*attP*) indicates circularization of the BV01 genome. Note that *attP* amplicons from Δ*int* + pNBU2-*int* are ~1.2 kb shorter than WT amplicons because of deletion of the integrase gene. Supernatant fractions were DNase treated, eliminating all contaminating host genomic DNA, as demonstrated by lack of amplification of a host marker gene (16S rRNA). Despite an apparent size shift of BVU_RS14350 amplicons from the pellets and supernatants, Sanger sequencing validated that the products have no apparent insertions (Figure S1B). PCR amplicons were visualized by agarose gel electrophoresis alongside the New England Biolabs (NEB) 1-kb DNA ladder (BVU_RS14350, *attP*) or GeneRuler Express DNA ladder (16S rRNA); numbers are in kilobases.

eventually observed in all animals in all cages. The average frequency of transduction ranged from 1.9×10^{-6} to 3.6×10^{-9} per animal. Of 26 transductant isolates that were colony purified, all were confirmed by PCR to have gained BV01 integrated at the known *attB*. Further, a representative transductant isolate was confirmed by whole-genome sequencing (Tables S2 and S3). These results support our hypothesis that an unknown mammalian host factor is required for novel BV01 infection.

To confirm that the release of DNase-protected BV01 genomes from host cells is a phage-encoded process, we sought to identify the phage integrase. BV01 encodes three genes with integrase domains (PF00589). We hypothesized that the gene BVU_RS14130, adjacent to the phage attachment site, was the most likely candidate for catalyzing integration and excision of BV01, as is common in phages (Casjens, 2003). A BVU_RS14130 deletion mutant (Δ*int*) was constructed (Figure 1A), and its activity was assayed by PCR of paired cell pellets and culture supernatants (Figure 2B). Phage DNA was not detected in the supernatants of the Δ*int* strain. Furthermore, the Δ*int* mutant did not yield an amplicon for circularization of BV01. Expression of the *int* gene in *trans* complements the circularization and release phenotypes (Figure 2B). These results demonstrate that the integrase encoded by BVU_RS14130 is necessary for phage excision, circularization, and release from the host. Furthermore, they suggest that BV01 is an intact prophage that directs its own mobilization.

Lysogeny with BV01 Alters the Host Transcriptome

We hypothesized that lysogeny with a prophage such as BV01 could alter the activities of the *B. vulgatus* host. RNA sequencing (RNA-seq) of the *B. vulgatus* WT lysogen and the isogenic cured lysogen was performed to identify transcripts differentially regulated in response to lysogeny (Figure 3). Our expectation was that if prophage BV01 modulates bacterial activities, then some of those changes would be apparent as changes in host gene expression.

Analysis of the RNA-seq data revealed 115 host transcripts differentially regulated in response to lysogeny with BV01 (Figure 3A), 103 of which (89%) were upregulated in the cured lysogen (Table S5). Resequencing of mutant genomes did not

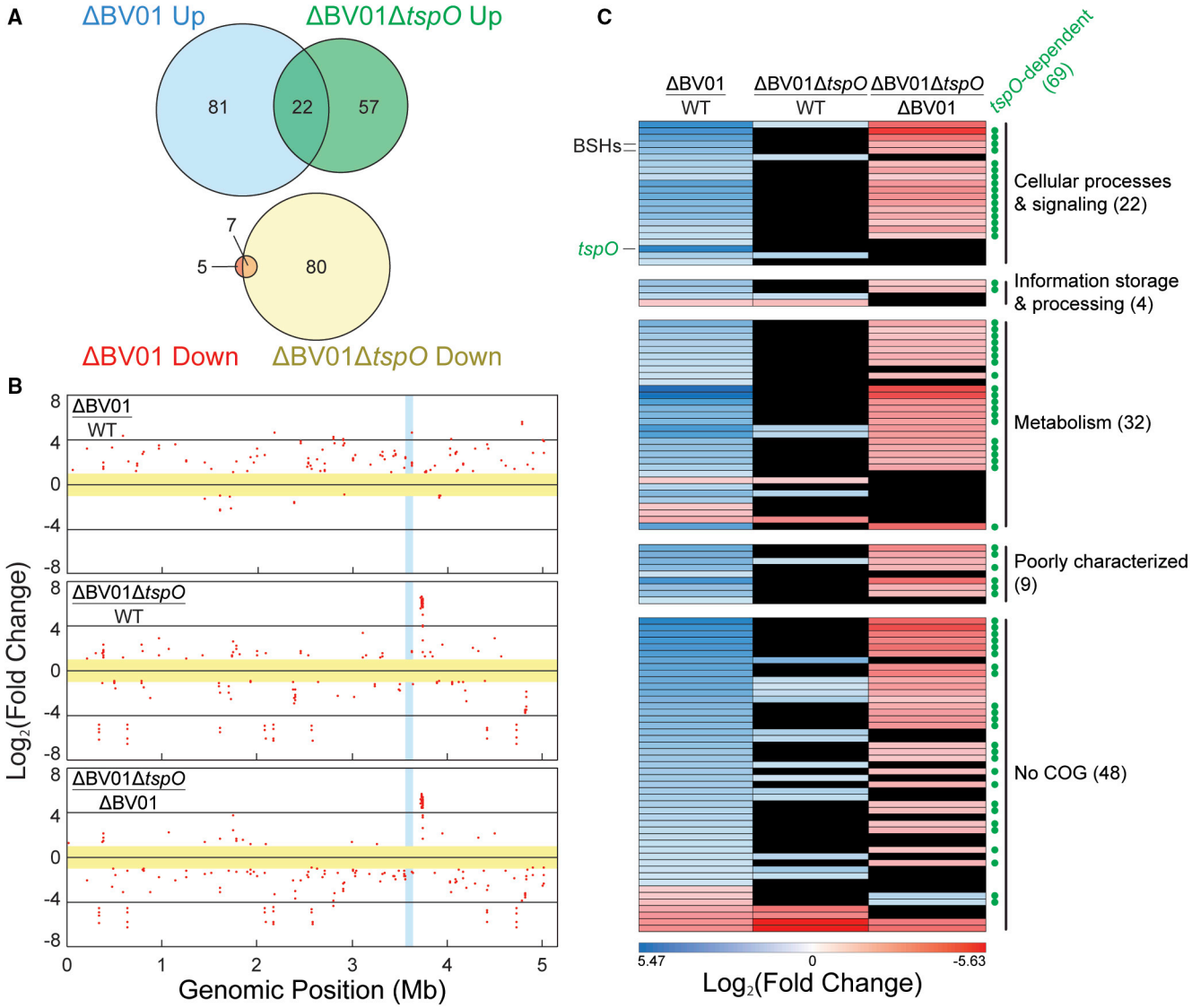

Figure 3. Differential Regulation of the Host Transcriptome in Response to BV01 Lysogeny

RNA-seq was performed in triplicate on the *B. vulgatus* WT lysogen, cured lysogen (ΔBV01), and *tspO* deletion cured lysogen (ΔBV01Δ*tspO*) strains at early log phase.

(A) Count of differentially regulated transcripts compared with the WT *B. vulgatus* lysogen (fold change ≥ 2, $q \leq 0.01$).

(B) Chromosomal location of the differentially expressed genes ($q \leq 0.01$). Each dot represents a differentially expressed transcript on a $\log_2$ scale; genes below the 2-fold change cutoff (yellow) and within the BV01 prophage (blue) are not shown. Positive fold change values correspond to ratios above 1 for each comparison.

(C) Functional assignment of 115 genes differentially expressed between WT and cured lysogen strains (fold change ≥ 2, $q \leq 0.01$). The locations of *tspO* and two bile salt hydrolases (BSHs) are indicated. General functions were assigned using the Clusters of Orthologous Groups (COGs); full functional categories are listed in Table S5. Transcripts that are not differentially expressed in other strain comparisons are shown in black. *tspO*-dependent transcripts are marked with green circles on the right.

reveal any secondary mutations likely to contribute to this global transcriptional response (Tables S2 and S3). These transcriptional changes occur across the host genome (Figure 3B). Functional analysis of these transcripts revealed that most function in metabolism and cellular processes and signaling (Figure 3C). However, pathway analysis using the Kyoto Encyclopedia of Genes and Genomes Pathway Database (Kanehisa and Goto, 2000) failed to yield pathway-level differences, which may be reflective of the level of annotation of the *B. vulgatus* genome. Taken together, these results indicate broad repression of a diverse array of host metabolic activities in response to prophage BV01, suggesting that it acts through one or more transcriptional regulators.

One possible explanation for the widespread transcriptomic response to BV01 lysogeny (Figure 3B) is that a phage product directly alters the transcriptional activity of host genes. BV01

encodes three candidate genes that might act in this way: a predicted phage repressor (BVU_RS14475), anti-repressor (BVU_RS14135), and sigma factor-like protein (BVU_RS14235) (Figure S1A). The putative phage repressor encoded by BVU_RS14475 is the most highly transcribed gene in the BV01 prophage, which might also interact with host promoters. Transcription of BVU_RS14135 and BVU_RS14235 is very low, so they are less likely to play a major role in the observed transcriptional response (Figure S1A). It is also possible that the observed transcriptional response to BV01 is the result of a host response to infection. A host-encoded, universal stress protein (*uspA*) homolog (BVU_RS16570) is upregulated in the BV01 lysogen (Table S5), but it is unknown whether that is a direct or indirect effect of infection.

BV01 Disruption of the *tspO* Promoter Alters Bile Acid Metabolism

Notably, integration of BV01 at *attB* is associated with a 23-fold downregulation of the adjacent downstream transcript (BVU_RS14490) encoding a predicted tryptophan-rich sensory protein (TspO). We hypothesized that this downregulation is caused by disruption of the *tspO* promoter because BV01 integrates between the predicted promoter and the ORF (Figure 4A). A low level of expression of this gene is observed in the WT lysogen, perhaps a result of readthrough from phage transcripts. TspO is an intramembrane protein whose endogenous ligand is unknown but that is broadly implicated in metabolic regulation and stress response in other bacteria (Balsemão-Pires et al., 2011; Davey and de Bruijn, 2000; Yeliseev and Kaplan, 1999). Sequence conservation specifically in the unstructured loop (LP1) and the cholesterol recognition/interaction amino acid consensus (CRAC) sequence of TspO suggest that the *B. vulgatus* copy may function similar to other bacterial copies (Guo et al., 2015; Li et al., 2015a; Zeno et al., 2012; Figure 4B). Although TspO is conserved in many bacteria, archaea, and eukaryotes, it is considered an accessory protein. Indeed, not all gut-associated members of the family Bacteroidales or the genus *Bacteroides* encode *tspO* (Figure 4C). Within *Bacteroides*, *tspO* is restricted to the clade that includes *B. vulgatus*, and among *B. vulgatus* strains, TspO is highly conserved (Figure 4D). Together, this suggests that TspO might play a specialized role in the lifestyle of *B. vulgatus*.

Given TspO's important role in regulating cellular activities in other bacterial systems, we hypothesized that it may be responsible for some of the differential regulation observed in response to BV01 lysogeny. A *tspO* deletion mutant was constructed in the cured lysogen background (ΔBV01Δ*tspO*), and its transcriptome was sequenced alongside that of the WT and cured lysogen strains (Figure 3). The predicted *tspO* regulon extends beyond the differential expression observed in the cured lysogen (Figures 3A and 3B), suggesting that the small amount of *tspO* transcription in the BV01 lysogen exerts effects on the rest of the transcriptome (Table S5).

Transcripts differentially regulated between the BV01 WT lysogen and cured lysogen that returned to WT-like levels upon further deletion of *tspO* were classified as *tspO*-dependent transcripts (Figure 3C). *TspO*-dependent transcripts are not significantly different in a ΔBV01Δ*tspO*/WT comparison because *tspO* is absent or minimally active under both of these conditions. Of the 115 transcripts differentially regulated in response to BV01, 69 (60%) are *tspO*-dependent. Of these 69 *tspO*-dependent genes, 67 are downregulated by BV01 integration (i.e., positive fold change for ΔBV01/WT) and downregulated by *tspO* deletion (i.e., negative fold change for ΔBV01Δ*tspO*/ΔBV01), suggesting that *tspO* is largely involved in activation of downstream transcripts.

How TspO, a membrane protein, affects downstream transcription is unknown (Davey and de Bruijn, 2000; Liu et al., 2006; Yeliseev and Kaplan, 1999). However, we hypothesize that, in *B. vulgatus*, like in other bacterial models, TspO is involved in a signaling cascade, possibly by transporting unknown ligands across the membrane or by interacting with other membrane proteins (Davey and de Bruijn, 2000; Liu et al., 2006; Yeliseev and Kaplan, 1999). Consistent with TspO's role in regulating stress, many *tspO*-dependent transcripts fall into the Clusters of Orthologous Groups (COG) category for post-translational modification, protein turnover, and chaperones, including several thioredoxins, peroxidases, and protein chaperones. *TspO*-dependent transcripts also account for the majority of metabolic genes differentially regulated in response to BV01 (Table S5).

Two *tspO*-dependent transcripts that are downregulated in response to lysogeny with BV01 encode putative bile salt hydrolases (BSHs; BVU_RS13575, 5.38-fold change, $q < 10^{-100}$; BVU_RS20010, 6.58-fold change, $q < 10^{-200}$) (Table S5). It was hypothesized that these transcriptional differences would reflect enzyme activities. To this end, *B. vulgatus* strains were grown in the presence of bile acids, and the deconjugation of those bile acids was measured by liquid chromatography-mass spectrometry (LC-MS) (Figure 5).

The LC-MS results show that the WT *B. vulgatus* lysogen does not significantly deconjugate glycocholic acid (GCA) to cholic acid (CA) and may exhibit modest deconjugation of taurocholic acid (TCA) (Figure 5; Figure S2). This agrees with a previous study that showed that *B. vulgatus* ATCC 8482 can deconjugate TCA but not GCA over a 48-h incubation (Yao et al., 2018). Importantly, CA is clearly detectable only in the cured lysogen background, consistent with the RNA-seq data (Figures 5A and 5B). This bile acid deconjugation phenotype is ablated with deletion of *tspO*, further supporting our hypothesis that *tspO* activates transcription of BSHs via an unknown mechanism, resulting in increased enzymatic activity (Figure 5C). Finally, resequencing of mutant genomes revealed no additional mutations likely to cause the restoration of BSH activity (Tables S2 and S3).

To see whether *tspO*-disrupted lysogens occur in natural human gut microbiomes, read mapping from 246 healthy human gut metagenomes was performed. Starting with reads that mapped to *tspO* in the reverse orientation, read mates were checked for mapping to phage BV01 and its relatives (Figure 6). All samples had reads mapping to *tspO*, with an average of 0.0004% of metagenome reads mapping, indicating that the corresponding population of *B. vulgatus* and *B. dorei* encoding *tspO* is relatively abundant (Figure S3A). Incidence of *tspO* associated with BV01 or a related phage is also common; 13.3% of samples (n = 34) contained read pairs mapping to *tspO* and an adjacent

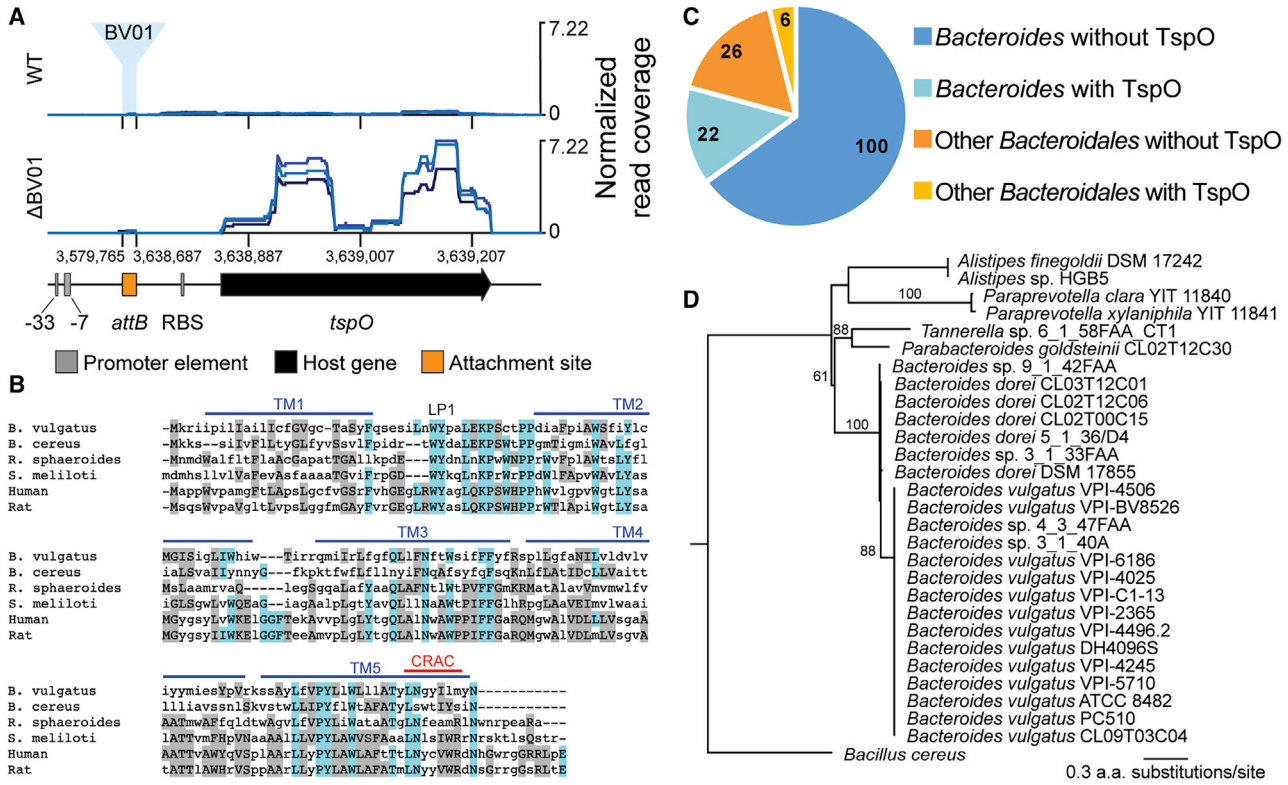

Figure 4. BV01 Integration Disrupts Transcription of *tspO*

(A) Transcriptional activity of the *tspO* gene region as it exists in the cured lysogen background. Locations of *tspO*, its predicted promoter elements (Bayley et al., 2000), and the empty BV01 *attB* are shown. RNA-seq read mapping from WT and ΔBV01 *B. vulgatus* was normalized to the total number of reads mapping to the genome. Three replicates are shown.

(B) Amino acid alignment of *B. vulgatus* TspO with known TspO sequences was generated with MUSCLE (Edgar, 2004). Identical and similar residues are colored blue and gray, respectively. Shown are TspO protein sequences from *B. vulgatus* (Refseq: WP_005843416.1), *Bacillus cereus* (GenBank: GCF80909.1), *Rhodobacter sphaeroides* (GenBank: AAF24291.1), *Sinorhizobium meliloti* (GenBank: AAF01195.1), human (RefSeq: NP_001243460.1), and rat (RefSeq: NP_036647.1). Transmembrane (TM) domains, the unstructured loop (LP), and the cholesterol recognition/interaction amino acid consensus (CRAC) sequence from *R. sphaeroides* TspO crystal structure are shown (Li et al., 2015a).

(C) The search for TspO homologs in the family Bacteroidales was accomplished with a BLAST-based approach using the *B. cereus* TspO (GenBank: GCF80909.1) as a query against a database of 154 gut-associated Bacteroidales genomes, 122 of which are in the genus *Bacteroides*. Genome counts are indicated.

(D) Gene tree estimated from TspO sequences across the Bacteroidales. All *B. vulgatus* and *B. dorei* genomes included in the search encode *tspO*. The clade for *B. vulgatus* TspO sequences is displayed as a polytomy; all *B. vulgatus* TspO sequences are at least 98% identical to each other. Numbers above branches represent bootstrap values; bootstraps over 50 are shown. The gene tree was estimated with FastTree (Price et al., 2010).

prophage. Within an individual microbiome, incidence of *tspO*-disrupted lysogens appears to be rare, usually comprising 3% or less of the combined *B. vulgatus* and *B. dorei* population, although, for some individuals, this incidence rate can be more than 10% (Figure S3B). Together, these data suggest that BV01 and other phages' effects on downstream phenotypes via *tspO* are likely quite common among humans, although these lysogens comprise the minority of the overall microbiome.

BV01 Represents the Proposed Virus Family Salyersviridae

While searching for potential new hosts for BV01, its predicted 25-bp *attB* was queried against 154 gut-associated Bacteroidales genomes. It was found that all *Paraprevotella* and *Bacteroides* genomes had at least the first 21 bases of the attachment site conserved (Figure 6A). In 20 genomes, two copies of the *att* site were found, and all were associated with putative prophages. In all instances, the putative *attL* and *attR* sites are direct repeats, as is true for BV01. Importantly, only *B. vulgatus* lysogens encode *tspO* (Figure 4); other prophages and *attB* sites occur in alternate genomic contexts. Alignment of these putative prophage-associated *att* sites finds that the first 22 bp are always conserved and that an additional 3 bp are variable among lysogen genomes (Figure 6B).

Integration at the same *att* site suggests that these prophages are genetically related. To assess relatedness, the Virus Classification and Tree Building Online Resource (VICTOR) (Meier-Kolthoff and Göker, 2017) was used to build a genome tree from all of the identified prophages (Figure 6C), and OPTSIL clustering (Göker et al., 2009) was used to predict taxonomic groups, which we named Salyersviridae, Salyersvirinae, and *Salyersvirus* (Table 1). Taxonomic clustering also defined phage species, four of which have more than one member. The species containing BV01 also contains BV02, a prophage 99.8%

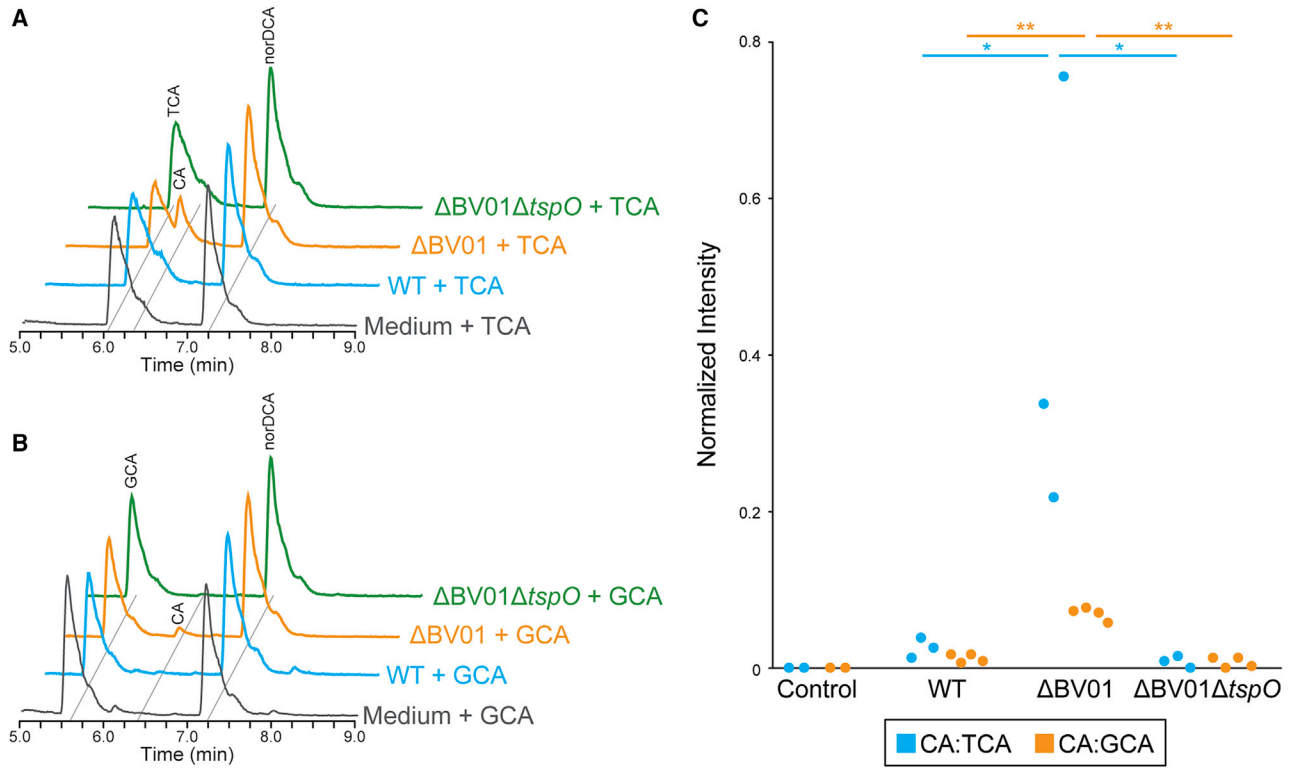

Figure 5. BV01 Alters Host Interactions with Bile Acids in a *tspO*-Dependent Manner

(A) Representative LC-MS traces showing that *B. vulgatus* deconjugates taurocholic acid (TCA) to cholic acid (CA) in the cured lysogen background (ΔBV01), but little or no CA is detectable in the WT or cured lysogen *tspO* deletion (ΔBV01Δ*tspO*) backgrounds. *B. vulgatus* cultures were incubated with 50 μM TCA for 16 h prior to bile acid extraction.

(B) Representative LC-MS traces showing that *B. vulgatus* deconjugates glycocholic acid (GCA) to CA in the ΔBV01 background but not in the WT or ΔBV01Δ*tspO* backgrounds. *B. vulgatus* cultures were incubated with 50 μM GCA for 48 h prior to bile acid extraction. Nordeoxycholic acid (norDCA) was added to a final concentration of 15 μM as an internal standard after incubation. Peaks were labeled for their metabolites based on m/z; TCA, 514.29; GCA, 464.30; CA, 407.28; norDCA, 377.27.

(C) Areas under the curve from extracted ion chromatograms were used to calculate relative intensity and averaged for CA:TCA (n = 3) and CA:GCA (n = 4) ratios. Statistical analyses were performed with one-way ANOVA; CA:TCA $df = 2$, $F = 6.59$, $p = 0.03$; CA:GCA $df = 3$, $F = 103.46$, $p < 0.0001$. Asterisks illustrate the Tukey's honestly significant difference test p value: *$p < 0.05$, **$p < 0.01$.

nucleotide identical to BV01. BV02 occurs in *B. vulgatus* VPI-4245, a strain cross-listed as ATCC 8482, suggesting that the BV01 prophage is ancestral to the strain lineage. Interestingly, the phage species BX01 has representatives in two distantly related hosts, *Bacteroides xylanisolvens* XB1A (phage BX01) and *B. thetaiotaomicron* 1_1_6 (phage BT01), suggesting that at least some salyersviruses have broad host ranges. Phage BC01 was placed outside of the subfamily Salyersvirinae, which is consistent with its considerable sequence divergence (Figure S4). Further examination of the BC01 *attL* and *attR* sites found that the 22-bp consensus sequence is only a portion of the full 69-bp repeat flanking the BC01 prophage, which further supports placement of BC01 outside of Salyersvirinae. Also included in the analysis were three known *Bacteroides*-infecting lytic phages: B124-14, B40-8, and crAssphage. OPTSIL taxonomic clustering placed phages B124-14 and B40-8 in the family Salyersviridae. This is consistent with an independent network analysis using vConTACT 2.0 (Bin Jang et al., 2019) and existing NCBI RefSeq viral genomes, which creates a cluster consisting of only BV01, B124-14, and B40-8. Similarities between Salyersviridae prophages and the two lytic phages are not detectable at the nucleotide sequence level (Figure S4A) but is likely driven by similarities in several proteins, including homologs to the predicted lysin, excisionase, and single-stranded DNA (ssDNA) binding protein from BV01 (Figure S4B).

To check that the proposed Salyersviridae clade was comprised of active phages, we searched for evidence of activity in culture and in wastewater samples. Sequencing and PCR were used to test the activity of six additional salyersviruses (Figure S5). Phages BV02, BV05, and BV06 were found to be released from host cells in culture, whereas BV03 is likely inactivated by genomic rearrangement (Figure S5D). We did not observe activity for BV04 or BO03 from *B. ovatus* ATCC 8483, both of which appear complete based on synteny with intact salyersviruses. This may be the result of inactivating mutations or not being induced under the growth conditions tested (Figure S5D).

Furthermore, we used read mapping to search for evidence of all 20 Salyersviridae phages in a wastewater metavirome

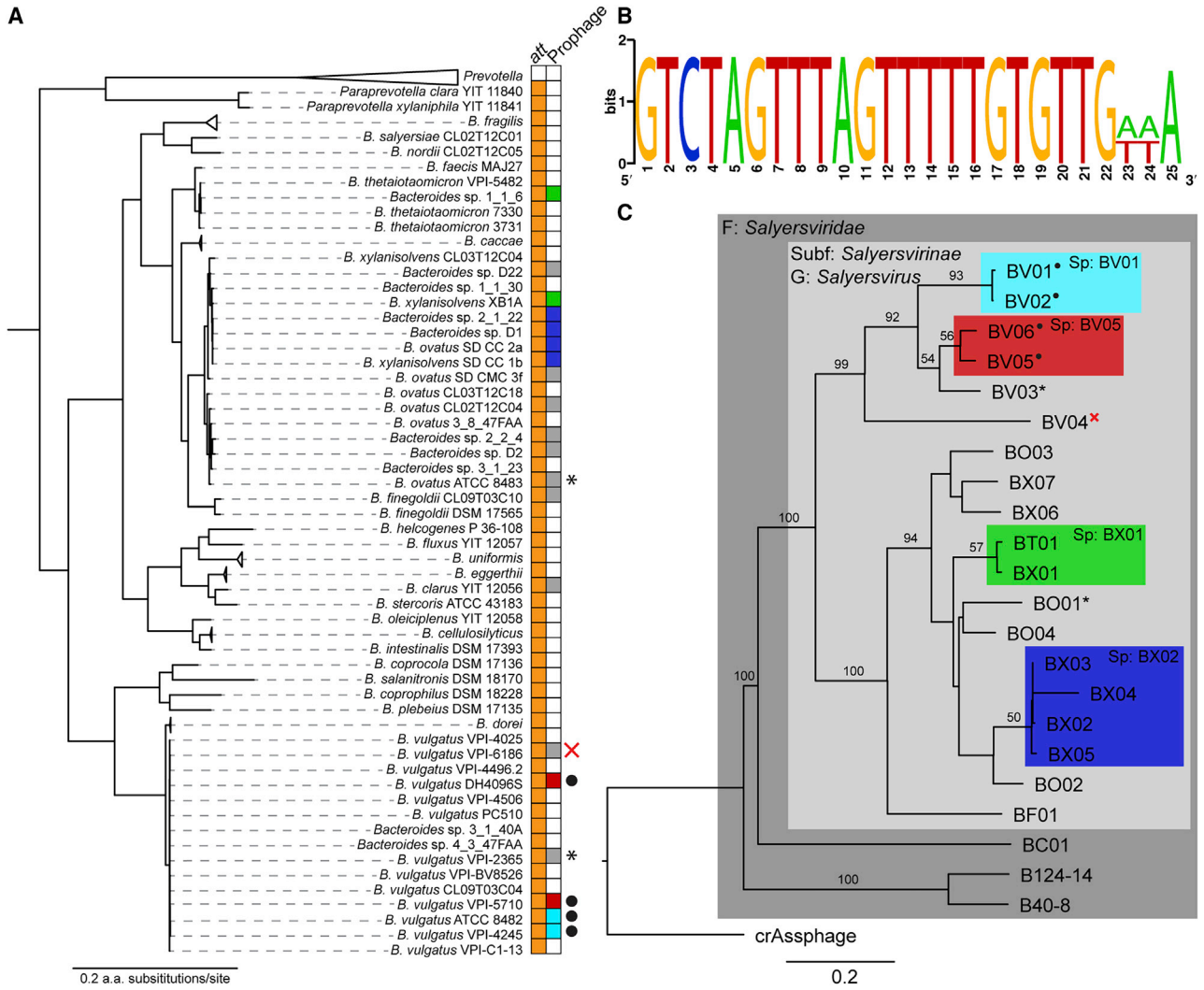

Figure 6. Salyersviridae Occur throughout the *Bacteroides* Genus

(A) *Bacteroides* phylogeny and occurrence of the Salyersviridae *att* site. All duplications of the *att* site are associated with a putative integrated prophage. Host phylogeny was estimated by maximum likelihood from concatenated alignment of 13 core genes.

(B) Consensus *att* site for Salyersvirinae. The *attP* is duplicated upon integration of a Salyersvirinae prophage, resulting in direct repeats. The image was made with the WebLogo online tool.

(C) Phylogenomic genome-BLAST distance phylogeny implemented with the VICTOR online tool (Meier-Kolthoff and Göker, 2017) using amino acid data from all phage ORFs. For consistency, all phage genomes were annotated with MetaGeneAnnotator (Noguchi et al., 2008) implemented via VirSorter (Roux et al., 2015). Support values above branches are Genome Blast Distance Phylogeny (GBDP) pseudo-bootstrap values from 100 replications. Family (F), subfamily (Subf), genus (G), and species (Sp) were assigned by OPTSIL clustering (Göker et al., 2009; Table 1). Each leaf of the tree represents a unique phage species, except where indicated by colored boxes. Active prophages were confirmed by sequencing and/or PCR, indicated by black dots; prophages confirmed to have been inactivated by genome rearrangement are indicated by an X; prophages that were tested for activity with inconclusive results are indicated by asterisks (Figure S4).

(Figure S5E). Reads mapped to all Salyersviridae genomes; however, it may be the result of sequence conservation within the family because reads often accumulate at the most conserved regions of each phage genome. Further, very little read mapping occurred in the distal portion of the inactivated prophage BV04, which resembles the host chromosome more than the phage sequence, indicating that virome processing removed most cellular DNA prior to sequencing (Figure S5E). *De novo* assembly of the individual wastewater viromes finds contigs that align with high identity but imperfectly to each Salyersviridae phage, supporting the findings seen by read mapping and suggesting that the real diversity of the family Salyersviridae is far greater than what has been observed to be integrated in cultured host genomes so far. This analysis found that phages infecting *B. vulgatus* are more abundant than other Salyersviridae phages based on maximum normalized read coverages. A similar comparison concludes that most individual temperate Salyersviridae phages are

Table 1. *Bacteroides* Phage Taxonomy as Determined by Whole-Genome Clustering

Phage	Host	Family	Subfamily	Genus	Species
BV01	*B. vulgatus* ATCC 8482	Salyersviridae	Salyersvirinae	*Salyersvirus*	*BV01*
BV02	*B. vulgatus* VPI-4245	Salyersviridae	Salyersvirinae	*Salyersvirus*	*BV01*
BV03	*B. vulgatus* VPI-2365	Salyersviridae	Salyersvirinae	*Salyersvirus*	*BV03*
BV04	*B. vulgatus* VPI-6186	Salyersviridae	Salyersvirinae	*Salyersvirus*	*BV04*
BV05	*B. vulgatus* VPI-5710	Salyersviridae	Salyersvirinae	*Salyersvirus*	*BV05*
BV06	*B. vulgatus* DH4096S	Salyersviridae	Salyersvirinae	*Salyersvirus*	*BV06*
BF01	*B. finegoldii* CL09T03C10	Salyersviridae	Salyersvirinae	*Salyersvirus*	*BF01*
BT01	*Bacteroides* sp. 1_1_6	Salyersviridae	Salyersvirinae	*Salyersvirus*	*BX01*
BO01	*B. ovatus* ATCC 8483	Salyersviridae	Salyersvirinae	*Salyersvirus*	*BO01*
BO02	*B. ovatus* CL02T12C04	Salyersviridae	Salyersvirinae	*Salyersvirus*	*BO02*
BO03	*Bacteroides* sp. 2_2_4	Salyersviridae	Salyersvirinae	*Salyersvirus*	*BO03*
BO04	*Bacteroides* sp. D2	Salyersviridae	Salyersvirinae	*Salyersvirus*	*BO04*
BX01	*B. xylanisolvens* XB1A	Salyersviridae	Salyersvirinae	*Salyersvirus*	*BX01*
BX02	*Bacteroides* sp. D1	Salyersviridae	Salyersvirinae	*Salyersvirus*	*BX02*
BX03	*Bacteroides* sp. 2_1_22	Salyersviridae	Salyersvirinae	*Salyersvirus*	*BX02*
BX04	*B. ovatus* SD. CC 2a	Salyersviridae	Salyersvirinae	*Salyersvirus*	*BX02*
BX05	*B. xylanisolvens* SD. CC 1b	Salyersviridae	Salyersvirinae	*Salyersvirus*	*BX02*
BX06	*Bacteroides* sp. D22	Salyersviridae	Salyersvirinae	*Salyersvirus*	*BX06*
BX07	*B. ovatus* SD. CMC 3f	Salyersviridae	Salyersvirinae	*Salyersvirus*	*BX07*
BC01	*B. clarus* YIT 12056	Salyersviridae	?	?	*BC01*
B124-14	*B. fragilis*	Salyersviridae	?	?	*B124-14*
B40-8	*B. fragilis*	Salyersviridae	?	?	*B40-8*
crAssphage	*B. intestinalis*	?	?	?	?

approximately equal in abundance to the lytic Salyersviridae phages B124-14 and B40-8 and approximately 10-fold less abundant than crAssphage in these wastewater viromes (Figure S5E). Searches for Salyersviridae phages in individual healthy human fecal metagenomes refine this conclusion, showing that, in most human samples, Salyersviridae phages are at least as abundant as crAssphage, although crAssphage can reach very high abundance in a subset of individuals (Figure S5F; Table S6). Although confirmation of most Salyersviridae activities and functions will require better sampling and *in vitro* testing, these results indicate that the phage family is active in human-associated communities.

DISCUSSION

Here we characterize a unique phage-host interaction between Bacteroides phage BV01 and its host *B. vulgatus.* We first demonstrate that BV01 is an intact prophage capable of directing its own excision and that it is transducible *in vivo* in a gnotobiotic mouse model. Using a combination of genetics, RNA-seq, and analytical chemistry, we show that BV01 decreases its host's ability to deconjugate bile acids by disrupting transcription of the gene adjacent to the *attB* encoding a TspO homolog. Furthermore, we show that *tspO* disruption by phage integration is common among, but rare within, healthy human gut microbiomes and can be mediated by BV01 or its relatives. Together, these findings elucidate a complex mechanism by which a phage alters its host's activities.

Repression of bile acid deconjugation as a consequence of BV01 integration is particularly relevant in the context of the mammalian gut. Mammals secrete conjugated primary bile acids into the small intestine, where they reach concentrations as high as 1 mM (Northfield and McColl, 1973); although the majority of bile acids secreted into the small intestine are reabsorbed, they can still accumulate to concentrations of 0.2–1 mM in the colon (Hamilton et al., 2007). Although bile acids are broadly capable of damaging lipid membranes, *Bacteroides* species are generally considered bile resistant (Citron et al., 1990), the mechanism of which is unknown. Bile acid deconjugation is a common activity encoded by gut-associated microbes, although its direct benefit to those microbes is unclear. Microbial modification of the bile acid pool can be linked to beneficial changes in the human host metabolism (Joyce et al., 2014; Yao et al., 2018) and varied epithelial susceptibility to viral pathogens (Grau et al., 2020). The link between BV01 and bile acid metabolism suggests a so far undescribed mechanism by which gut phages might influence mammalian host phenotypes.

Here, bile acid deconjugation in *B. vulgatus* is dependent on a putative TspO. Bacterial TspOs are important for regulating metabolic switches and stress regulation in at least three diverse systems (Balsemão-Pires et al., 2011; Davey and de Bruijn, 2000; Yeliseev and Kaplan, 1999), but the mechanism of action for the protein is unknown. The crystal structure of TspO shows a periplasm-facing binding pocket distinct from the intramembrane cholesterol recognition consensus sequence, which may bind or degrade porphyrins (Guo et al., 2015; Li et al., 2015a;

Zeno et al., 2012). The porphyrin degrading and cholesterol transporting functions of TspO, however, have been disputed (Li et al., 2015b; Rone et al., 2012). Despite this, it is notable that cholesterol is structurally similar to bile acids, being their biosynthetic precursor. In at least one other gut-associated microbe, *tspO* is upregulated by bile acids, suggesting that TspO may be involved more broadly in bile acid metabolism in gut microbes (Devendran et al., 2019). The regulatory link described here between bile acid hydrolysis and TspO suggests a hypothesis where the *B. vulgatus* TspO might be a sensor and regulator of bile acid interactions.

Induction of BV01 from its integrated state and infection of new hosts remains enigmatic. Prophage induction is canonically linked to stress-dependent pathways, as in lambdoid phages that respond to DNA damage via RecA-dependent cleavage of the CI repressor protein (Roberts et al., 1978). It is possible that prophages in *Bacteroides* hosts respond to alternative stimuli, as is the case for CTnDOT, a well-studied *Bacteroides* conjugative transposon whose excision is inducible only by tetracycline (Moon et al., 2005). Neither DNA damage nor antibiotics induce prophage BV01 *in vitro*, so all experiments here relied on an apparently low rate of spontaneous prophage induction. Similarly, no infection conditions or susceptible hosts have been identified for BV01 *in vitro*. We demonstrate that BV01 is transducible in a gnotobiotic mouse model, suggesting that an unknown mammalian host factor is required for novel BV01 infection. Enigmatic infection dynamics may be a result of the phase-variable polysaccharide capsule; recent work suggests that heterogeneity in capsule composition hinders phage infection on population scales (Porter et al., 2020). Indeed, it has long been observed that finding phages in *Bacteroides* using traditional techniques is difficult or impossible for most host strains (Puig and Gironés, 1999; Salyers et al., 2000), making the host-first approach to phage discovery used here especially appealing.

Finally, phage BV01 is the first explored representative of the broad family Salyersviridae, which spans an entire host genus and includes lytic and temperate members. Salyersviridae is common and diverse among natural human samples but rare within individuals, suggesting that lysogenization may confer frequency-dependent advantages to the bacterial host. The genetic context of non-*B. vulgatus* Salyersviridae lysogens remains unexplored and likely underlies different phage-host interactions. The absence of *tspO* in these other host systems may provide the ideal background for studying more direct effects on the bacterial host. Certainly, other interactions between BV01 and its host remain to be studied, although they were overshadowed here by the enormous effects of *tspO*. Future studies should also examine the role of Salyersviridae phages on bacterial host fitness and evolution (Oh et al., 2019; Zhao et al., 2019) because these phages likely have important ripple effects throughout the microbiome and on the mammalian host that remain to be elucidated.

STAR★METHODS

Detailed methods are provided in the online version of this paper and include the following:

SUPPLEMENTAL INFORMATION

Supplemental Information can be found online at https://doi.org/10.1016/j.celrep.2020.108142.

ACKNOWLEDGMENTS

We thank Nadja Shoemaker and Abigail Salyers for access to an impressive collection of *Bacteroides* isolates, Ken Ringwald for critical review of the manuscript, Jim Imlay for insightful discussions regarding metabolism and stress, Alvaro Hernandez and Chris Wright for DNA and RNA sequencing, Bruce Rabe for aid with wastewater collection, Jonathan Mitchell for maintenance and animal care at the UCR vivarium, Jericho Ortanez for assistance with construction of pNBU2-*bla-cfx*, and Nicholas Zanghi for assistance with construction of the Δ*int* mutant. This research was supported by initial complement funding to P.H.D. from the University of Illinois at Urbana-Champaign (UIUC) and the University of California, Riverside (UCR), and D.E.C. was supported by the UIUC Department of Microbiology. L.K.L. was supported by a National Science Foundation graduate research fellowship. Gnotobiotic mouse work and A.H. were supported by National Institute of General Medical Sciences grant R35GM124724. R.J.W. is supported by the Allen Foundation with an Allen Distinguished Investigator Award.

AUTHOR CONTRIBUTIONS

Conceptualization, D.E.C., R.J.W., and P.H.D.; Methodology, D.E.C., L.K.L., J.M.R., A.H., R.J.W., and P.H.D.; Software, D.E.C. and P.H.D.; Validation, D.E.C.; Formal Analysis, D.E.C. and P.H.D.; Investigation, D.E.C. and P.H.D.; Resources, J.M.R., A.H., R.J.W., and P.H.D.; Data Curation, D.E.C. and P.H.D.; Writing—Original Draft, D.E.C.; Writing—Review and Editing, D.E.C., L.K.L., J.M.R., A.H., R.J.W., and P.H.D.; Visualization, D.E.C., L.K.L., and P.H.D.; Supervision, J.M.R., R.J.W., and P.H.D.; Project Administration, D.E.C. and P.H.D.; Funding Acquisition, R.J.W. and P.H.D.

DECLARATION OF INTERESTS

The authors declare no competing interests.

Received: April 10, 2020
Revised: July 7, 2020
Accepted: August 21, 2020
Published: September 15, 2020

SUPPORTING CITATIONS

The following references appear in the Supplemental Information: Caporaso et al. (2011), Eggerth and Gagnon (1933), Johnson (1978), Shoemaker et al. (2001), Simon et al. (1983), Whittle et al. (2001).

REFERENCES

Abeles, S.R., Ly, M., Santiago-Rodriguez, T.M., and Pride, D.T. (2015). Effects of long term antibiotic therapy on human oral and fecal viromes. PLoS ONE *10*, e0134941.

Almagro Armenteros, J.J., Tsirigos, K.D., Sønderby, C.K., Petersen, T.N., Winther, O., Brunak, S., von Heijne, G., and Nielsen, H. (2019). SignalP 5.0 improves signal peptide predictions using deep neural networks. Nat. Biotechnol. *37*, 420–423.

Anantharaman, K., Duhaime, M.B., Breier, J.A., Wendt, K.A., Toner, B.M., and Dick, G.J. (2014). Sulfur oxidation genes in diverse deep-sea viruses. Science *344*, 757–760.

Balsemão-Pires, E., Jaillais, Y., Olson, B.J., Andrade, L.R., Umen, J.G., Chory, J., and Sachetto-Martins, G. (2011). The *Arabidopsis* translocator protein (AtTSPO) is regulated at multiple levels in response to salt stress and perturbations in tetrapyrrole metabolism. BMC Plant Biol. *11*, 108.

Bateman, A., Coin, L., Durbin, R., Finn, R.D., Hollich, V., Griffiths-Jones, S., Khanna, A., Marshall, M., Moxon, S., Sonnhammer, E.L.L., et al. (2004). The Pfam protein families database. Nucleic Acids Res. *32*, D138–D141.

Baugher, J.L., Durmaz, E., and Klaenhammer, T.R. (2014). Spontaneously induced prophages in *Lactobacillus gasseri* contribute to horizontal gene transfer. Appl. Environ. Microbiol. *80*, 3508–3517.

Bayley, D.P., Rocha, E.R., and Smith, C.J. (2000). Analysis of *cepA* and other *Bacteroides fragilis* genes reveals a unique promoter structure. FEMS Microbiol. Lett. *193*, 149–154.

Bensing, B.A., Siboo, I.R., and Sullam, P.M. (2001). Proteins PblA and PblB of *Streptococcus mitis*, which promote binding to human platelets, are encoded within a lysogenic bacteriophage. Infect. Immun. *69*, 6186–6192.

Benson, D.A., Karsch-Mizrachi, I., Lipman, D.J., Ostell, J., and Sayers, E.W. (2009). GenBank. Nucleic Acids Res. *37*, D26–D31.

Berger, P., Kouzel, I.U., Berger, M., Haarmann, N., Dobrindt, U., Koudelka, G.B., and Mellmann, A. (2019). Carriage of Shiga toxin phage profoundly affects *Escherichia coli* gene expression and carbon source utilization. BMC Genomics *20*, 504.

Bin Jang, H., Bolduc, B., Zablocki, O., Kuhn, J.H., Roux, S., Adriaenssens, E.M., Brister, J.R., Kropinski, A.M., Krupovic, M., Lavigne, R., et al. (2019). Taxonomic assignment of uncultivated prokaryotic virus genomes is enabled by gene-sharing networks. Nat. Biotechnol. *37*, 632–639.

Bolger, A.M., Lohse, M., and Usadel, B. (2014). Trimmomatic: a flexible trimmer for Illumina sequence data. Bioinformatics *30*, 2114–2120.

Bonanno, L., Petit, M.-A., Loukiadis, E., Michel, V., and Auvray, F. (2016). Heterogeneity in induction level, infection ability, and morphology of Shiga toxin-encoding phages (Stx Phages) from dairy and human Shiga toxin-producing *Escherichia coli* O26:H11 isolates. Appl. Environ. Microbiol. *82*, 2177–2186.

Bondy-Denomy, J., and Davidson, A.R. (2014). When a virus is not a parasite: the beneficial effects of prophages on bacterial fitness. J. Microbiol. *52*, 235–242.

Caporaso, J.G., Lauber, C.L., Walters, W.A., Berg-Lyons, D., Lozupone, C.A., Turnbaugh, P.J., Fierer, N., and Knight, R. (2011). Global patterns of 16S rRNA diversity at a depth of millions of sequences per sample. Proc. Natl. Acad. Sci. USA *108* (*Suppl 1*), 4516–4522.

Carey, J.N., Mettert, E.L., Fishman-Engel, D.R., Roggiani, M., Kiley, P.J., and Goulian, M. (2019). Phage integration alters the respiratory strategy of its host. eLife *8*, e49081.

Carver, T., Harris, S.R., Berriman, M., Parkhill, J., and McQuillan, J.A. (2012). Artemis: an integrated platform for visualization and analysis of high-throughput sequence-based experimental data. Bioinformatics *28*, 464–469.

Casjens, S. (2003). Prophages and bacterial genomics: what have we learned so far? Mol. Microbiol. *49*, 277–300.

Chen, Y.Y., Wang, J.T., Lin, T.L., Gong, Y.N., Li, T.H., Huang, Y.Y., and Hsieh, Y.C. (2019). Prophage excision in *Streptococcus pneumoniae* serotype 19A ST320 promote colonization: Insight into its evolution from the ancestral clone Taiwan 19F-14 (ST236). Front. Microbiol. *10*, 205.

Citron, D.M., Baron, E.J., Finegold, S.M., and Goldstein, E.J. (1990). Short prereduced anaerobically sterilized (PRAS) biochemical scheme for identification of clinical isolates of bile-resistant *Bacteroides* species. J. Clin. Microbiol. *28*, 2220–2223.

Coyne, M.J., Zitomersky, N.L., McGuire, A.M., Earl, A.M., and Comstock, L.E. (2014). Evidence of extensive DNA transfer between *Bacteroidales* species within the human gut. MBio *5*, e01305–e01314.

Cullen, T.W., Schofield, W.B., Barry, N.A., Putnam, E.E., Rundell, E.A., Trent, M.S., Degnan, P.H., Booth, C.J., Yu, H., and Goodman, A.L. (2015). Antimicrobial peptide resistance mediates resilience of prominent gut commensals during inflammation. Science *347*, 170–175.

Davey, M.E., and de Bruijn, F.J. (2000). A homologue of the tryptophan-rich sensory protein TspO and FixL regulate a novel nutrient deprivation-induced *Sinorhizobium meliloti* locus. Appl. Environ. Microbiol. *66*, 5353–5359.

Deatherage, D.E., and Barrick, J.E. (2014). Identification of mutations in laboratory-evolved microbes from next-generation sequencing data using breseq. Methods Mol. Biol. *1151*, 165–188.

Degnan, P.H., Taga, M.E., and Goodman, A.L. (2014). Vitamin B_{12} as a modulator of gut microbial ecology. Cell Metab. *20*, 769–778.

Devendran, S., Shrestha, R., Alves, J.M.P., Wolf, P.G., Ly, L., Hernandez, A.G., Méndez-García, C., Inboden, A., Wiley, J., Paul, O., et al. (2019). *Clostridium scindens* ATCC 35704: Integration of nutritional requirements, the complete genome sequence, and global transcriptional responses to bile acids. Appl. Environ. Microbiol. *85*, e00052–19.

Dutilh, B.E., Cassman, N., McNair, K., Sanchez, S.E., Silva, G.G.Z., Boling, L., Barr, J.J., Speth, D.R., Seguritan, V., Aziz, R.K., et al. (2014). A highly abundant bacteriophage discovered in the unknown sequences of human faecal metagenomes. Nat. Commun. *5*, 4498.

Edgar, R.C. (2004). MUSCLE: multiple sequence alignment with high accuracy and high throughput. Nucleic Acids Res. *32*, 1792–1797.

Eggerth, A.H., and Gagnon, B.H. (1933). The *Bacteroides* of human feces. J. Bacteriol. *25*, 389–413.

El Kaoutari, A., Armougom, F., Gordon, J.I., Raoult, D., and Henrissat, B. (2013). The abundance and variety of carbohydrate-active enzymes in the human gut microbiota. Nat. Rev. Microbiol. *11*, 497–504.

Feiner, R., Argov, T., Rabinovich, L., Sigal, N., Borovok, I., and Herskovits, A.A. (2015). A new perspective on lysogeny: prophages as active regulatory switches of bacteria. Nat. Rev. Microbiol. *13*, 641–650.

Göker, M., García-Blázquez, G., Voglmayr, H., Tellería, M.T., and Martín, M.P. (2009). Molecular taxonomy of phytopathogenic fungi: a case study in *Peronospora*. PLoS ONE *4*, e6319.

Goodman, A.L., McNulty, N.P., Zhao, Y., Leip, D., Mitra, R.D., Lozupone, C.A., Knight, R., and Gordon, J.I. (2009). Identifying genetic determinants needed to establish a human gut symbiont in its habitat. Cell Host Microbe *6*, 279–289.

Grau, K.R., Zhu, S., Peterson, S.T., Helm, E.W., Philip, D., Phillips, M., Hernandez, A., Turula, H., Frasse, P., Graziano, V.R., et al. (2020). The intestinal regionalization of acute norovirus infection is regulated by the microbiota via bile acid-mediated priming of type III interferon. Nat. Microbiol. *5*, 84–92.

Guo, Y., Kalathur, R.C., Liu, Q., Kloss, B., Bruni, R., Ginter, C., Kloppmann, E., Rost, B., and Hendrickson, W.A. (2015). Structure and activity of tryptophan-rich TSPO proteins. Science *347*, 551–555.

Haft, D.H., Selengut, J.D., and White, O. (2003). The TIGRFAMs database of protein families. Nucleic Acids Res. *31*, 371–373.

Hamilton, J.P., Xie, G., Raufman, J.-P., Hogan, S., Griffin, T.L., Packard, C.A., Chatfield, D.A., Hagey, L.R., Steinbach, J.H., and Hofmann, A.F. (2007). Human cecal bile acids: concentration and spectrum. Am. J. Physiol. Gastrointest. Liver Physiol. *293*, G256–G263.

Han, M., Yang, P., Zhong, C., and Ning, K. (2018). The human gut virome in hypertension. Front. Microbiol. *9*, 3150.

Hannigan, G.D., Duhaime, M.B., Ruffin, M.T., 4th, Koumpouras, C.C., and Schloss, P.D. (2018). Diagnostic potential and interactive dynamics of the colorectal cancer virome. MBio *9*, e02248–18.

Hernandez-Doria, J.D., and Sperandio, V. (2018). Bacteriophage transcription factor Cro regulates virulence gene expression in enterohemorrhagic *Escherichia coli*. Cell Host Microbe *23*, 607–617.e6.

Hickey, C.A., Kuhn, K.A., Donermeyer, D.L., Porter, N.T., Jin, C., Cameron, E.A., Jung, H., Kaiko, G.E., Wegorzewska, M., Malvin, N.P., et al. (2015). Colitogenic *Bacteroides thetaiotaomicron* antigens access host immune cells in a sulfatase-dependent manner via outer membrane vesicles. Cell Host Microbe *17*, 672–680.

Hills, R.D., Jr., Pontefract, B.A., Mishcon, H.R., Black, C.A., Sutton, S.C., and Theberge, C.R. (2019). Gut microbiome: profound implications for diet and disease. Nutrients *11*, 1613.

Howard-Varona, C., Hargreaves, K.R., Abedon, S.T., and Sullivan, M.B. (2017). Lysogeny in nature: mechanisms, impact and ecology of temperate phages. ISME J. *11*, 1511–1520.

Hsu, B.B., Gibson, T.E., Yeliseyev, V., Liu, Q., Lyon, L., Bry, L., Silver, P.A., and Gerber, G.K. (2019). Dynamic modulation of the gut microbiota and metabolome by bacteriophages in a mouse model. Cell Host Microbe *25*, 803–814.e5.

Hyatt, D., Chen, G.-L., Locascio, P.F., Land, M.L., Larimer, F.W., and Hauser, L.J. (2010). Prodigal: prokaryotic gene recognition and translation initiation site identification. BMC Bioinformatics *11*, 119.

Jermyn, W.S., and Boyd, E.F. (2002). Characterization of a novel *Vibrio* pathogenicity island (VPI-2) encoding neuraminidase (*nanH*) among toxigenic *Vibrio cholerae* isolates. Microbiology *148*, 3681–3693.

Jofre, J., Blanch, A.R., Lucena, F., and Muniesa, M. (2014). Bacteriophages infecting *Bacteroides* as a marker for microbial source tracking. Water Res. *55*, 1–11.

Johnson, J.L. (1978). Taxonomy of the *Bacteroides*. Int. J. Syst. Evol. Microbiol. *28*, 245–256.

Joyce, S.A., MacSharry, J., Casey, P.G., Kinsella, M., Murphy, E.F., Shanahan, F., Hill, C., and Gahan, C.G.M. (2014). Regulation of host weight gain and lipid metabolism by bacterial bile acid modification in the gut. Proc. Natl. Acad. Sci. USA *111*, 7421–7426.

Kanehisa, M., and Goto, S. (2000). KEGG: Kyoto Encyclopedia of Genes and Genomes. Nucleic Acids Res. *28*, 27–30.

Kelley, L.A., Mezulis, S., Yates, C.M., Wass, M.N., and Sternberg, M.J.E. (2015). The Phyre2 web portal for protein modeling, prediction and analysis. Nat. Protoc. *10*, 845–858.

Khan Mirzaei, M., Khan, M.A.A., Ghosh, P., Taranu, Z.E., Taguer, M., Ru, J., Chowdhury, R., Kabir, M.M., Deng, L., Mondal, D., and Maurice, C.F. (2020). Bacteriophages isolated from stunted children can regulate gut bacterial communities in an age-specific manner. Cell Host Microbe *27*, 199–212.e5.

Kongari, R., Rajaure, M., Cahill, J., Rasche, E., Mijalis, E., Berry, J., and Young, R. (2018). Phage spanins: diversity, topological dynamics and gene convergence. BMC Bioinformatics *19*, 326.

Koonin, E.V., and Yutin, N. (2020). The crAss-like phage group: how metagenomics reshaped the human virome. Trends Microbiol. *28*, 349–359.

Koropatkin, N.M., Martens, E.C., Gordon, J.I., and Smith, T.J. (2008). Starch catabolism by a prominent human gut symbiont is directed by the recognition of amylose helices. Structure *16*, 1105–1115.

Krinos, C.M., Coyne, M.J., Weinacht, K.G., Tzianabos, A.O., Kasper, D.L., and Comstock, L.E. (2001). Extensive surface diversity of a commensal microorganism by multiple DNA inversions. Nature *414*, 555–558.

Kropinski, A.M., Mazzocco, A., Waddell, T.E., Lingohr, E., and Johnson, R.P. (2009). Enumeration of bacteriophages by double agar overlay plaque assay. Methods Mol. Biol. *501*, 69–76.

Krupovic, M., and Forterre, P. (2011). Microviridae goes temperate: microvirus-related proviruses reside in the genomes of *Bacteroidetes*. PLoS ONE *6*, e19893.

Lagesen, K., Hallin, P., Rødland, E.A., Staerfeldt, H.-H., Rognes, T., and Ussery, D.W. (2007). RNAmmer: consistent and rapid annotation of ribosomal RNA genes. Nucleic Acids Res. *35*, 3100–3108.

Lange, A., Beier, S., Steimle, A., Autenrieth, I.B., Huson, D.H., and Frick, J.-S. (2016). Extensive mobilome-driven genome diversification in mouse gut-associated *Bacteroides vulgatus* mpk. Genome Biol. Evol. *8*, 1197–1207.

Leplae, R., Lima-Mendez, G., and Toussaint, A. (2010). ACLAME: a CLAssification of Mobile genetic Elements, update 2010. Nucleic Acids Res. *38*, D57–D61.

Li, H., and Durbin, R. (2009). Fast and accurate short read alignment with Burrows-Wheeler transform. Bioinformatics *25*, 1754–1760.

Li, F., Liu, J., Zheng, Y., Garavito, R.M., and Ferguson-Miller, S. (2015a). Protein structure. Crystal structures of translocator protein (TSPO) and mutant mimic of a human polymorphism. Science *347*, 555–558.

Li, F., Liu, J., Garavito, R.M., and Ferguson-Miller, S. (2015b). Evolving understanding of translocator protein 18 kDa (TSPO). Pharmacol. Res. *99*, 404–409.

Lima-Mendez, G., Van Helden, J., Toussaint, A., and Leplae, R. (2008). Prophinder: a computational tool for prophage prediction in prokaryotic genomes. Bioinformatics *24*, 863–865.

Liu, J., Rone, M.B., and Papadopoulos, V. (2006). Protein-protein interactions mediate mitochondrial cholesterol transport and steroid biosynthesis. J. Biol. Chem. *281*, 38879–38893.

Lowe, T.M., and Eddy, S.R. (1997). tRNAscan-SE: a program for improved detection of transfer RNA genes in genomic sequence. Nucleic Acids Res. *25*, 955–964.

McClure, R., Balasubramanian, D., Sun, Y., Bobrovskyy, M., Sumby, P., Genco, C.A., Vanderpool, C.K., and Tjaden, B. (2013). Computational analysis of bacterial RNA-Seq data. Nucleic Acids Res. *41*, e140.

Meier-Kolthoff, J.P., and Göker, M. (2017). VICTOR: genome-based phylogeny and classification of prokaryotic viruses. Bioinformatics *33*, 3396–3404.

Minot, S., Sinha, R., Chen, J., Li, H., Keilbaugh, S.A., Wu, G.D., Lewis, J.D., and Bushman, F.D. (2011). The human gut virome: inter-individual variation and dynamic response to diet. Genome Res. *21*, 1616–1625.

Mirzaei, M.K., and Maurice, C.F. (2017). Ménage à trois in the human gut: interactions between host, bacteria and phages. Nat. Rev. Microbiol. *15*, 397–408.

Monaco, C.L., Gootenberg, D.B., Zhao, G., Handley, S.A., Ghebremichael, M.S., Lim, E.S., Lankowski, A., Baldridge, M.T., Wilen, C.B., Flagg, M., et al. (2016). Altered virome and bacterial microbiome in Human Immunodeficiency Virus-associated Acquired Immunodeficiency Syndrome. Cell Host Microbe *19*, 311–322.

Moon, K., Shoemaker, N.B., Gardner, J.F., and Salyers, A.A. (2005). Regulation of excision genes of the *Bacteroides* conjugative transposon CTnDOT. J. Bacteriol. *187*, 5732–5741.

Moreno-Gallego, J.L., Chou, S.-P., Di Rienzi, S.C., Goodrich, J.K., Spector, T.D., Bell, J.T., Youngblut, N.D., Hewson, I., Reyes, A., and Ley, R.E. (2019). Virome diversity correlates with intestinal microbiome diversity in adult monozygotic twins. Cell Host Microbe *25*, 261–272.e5.

Mount, D.W. (2007). Using the Basic Local Alignment Search Tool (BLAST). CSH Protoc. *2007*, pdb.top17.

Nakayama, K., Kanaya, S., Ohnishi, M., Terawaki, Y., and Hayashi, T. (1999). The complete nucleotide sequence of φ CTX, a cytotoxin-converting phage

of *Pseudomonas aeruginosa*: implications for phage evolution and horizontal gene transfer via bacteriophages. Mol. Microbiol. *31*, 399–419.

Nawrocki, E.P., and Eddy, S.R. (2013). Infernal 1.1: 100-fold faster RNA homology searches. Bioinformatics *29*, 2933–2935.

Noguchi, H., Taniguchi, T., and Itoh, T. (2008). MetaGeneAnnotator: detecting species-specific patterns of ribosomal binding site for precise gene prediction in anonymous prokaryotic and phage genomes. DNA Res. *15*, 387–396.

Norman, J.M., Handley, S.A., Baldridge, M.T., Droit, L., Liu, C.Y., Keller, B.C., Kambal, A., Monaco, C.L., Zhao, G., Fleshner, P., et al. (2015). Disease-specific alterations in the enteric virome in inflammatory bowel disease. Cell *160*, 447–460.

Northfield, T.C., and McColl, I. (1973). Postprandial concentrations of free and conjugated bile acids down the length of the normal human small intestine. Gut *14*, 513–518.

Nurk, S., Meleshko, D., Korobeynikov, A., and Pevzner, P.A. (2017). metaSPAdes: a new versatile metagenomic assembler. Genome Res. *27*, 824–834.

Ogilvie, L.A., Bowler, L.D., Caplin, J., Dedi, C., Diston, D., Cheek, E., Taylor, H., Ebdon, J.E., and Jones, B.V. (2013). Genome signature-based dissection of human gut metagenomes to extract subliminal viral sequences. Nat. Commun. *4*, 2420.

Oh, J.H., Lin, X.B., Zhang, S., Tollenaar, S.L., Özçam, M., Dunphy, C., Walter, J., and van Pijkeren, J.-P. (2019). Prophages in *Lactobacillus reuteri* are associated with fitness trade-offs but can increase competitiveness in the gut ecosystem. Appl. Environ. Microbiol. *86*, e01922–19.

Patrick, S., Blakely, G.W., Houston, S., Moore, J., Abratt, V.R., Bertalan, M., Cerdeño-Tárraga, A.M., Quail, M.A., Corton, N., Corton, C., et al. (2010). Twenty-eight divergent polysaccharide loci specifying within- and amongst-strain capsule diversity in three strains of *Bacteroides fragilis*. Microbiology *156*, 3255–3269.

Planer, J.D., Peng, Y., Kau, A.L., Blanton, L.V., Ndao, I.M., Tarr, P.I., Warner, B.B., and Gordon, J.I. (2016). Development of the gut microbiota and mucosal IgA responses in twins and gnotobiotic mice. Nature *534*, 263–266.

Porter, N.T., Hryckowian, A.J., Merrill, B.D., Fuentes, J.J., Gardner, J.O., Glowacki, R.W.P., Singh, S., Crawford, R.D., Snitkin, E.S., Sonnenburg, J.L., and Martens, E.C. (2020). Phase-variable capsular polysaccharides and lipoproteins modify bacteriophage susceptibility in *Bacteroides thetaiotaomicron*. Nat. Microbiol. *5*, 1170–1181.

Price, M.N., Dehal, P.S., and Arkin, A.P. (2010). FastTree 2–approximately maximum-likelihood trees for large alignments. PLoS ONE *5*, e9490.

Puig, M., and Gironés, R. (1999). Genomic structure of phage B40-8 of *Bacteroides fragilis*. Microbiology *145*, 1661–1670.

Rabinovich, L., Sigal, N., Borovok, I., Nir-Paz, R., and Herskovits, A.A. (2012). Prophage excision activates *Listeria* competence genes that promote phagosomal escape and virulence. Cell *150*, 792–802.

Reyes, A., Wu, M., McNulty, N.P., Rohwer, F.L., and Gordon, J.I. (2013). Gnotobiotic mouse model of phage-bacterial host dynamics in the human gut. Proc. Natl. Acad. Sci. USA *110*, 20236–20241.

Reyes, A., Blanton, L.V., Cao, S., Zhao, G., Manary, M., Trehan, I., Smith, M.I., Wang, D., Virgin, H.W., Rohwer, F., and Gordon, J.I. (2015). Gut DNA viromes of Malawian twins discordant for severe acute malnutrition. Proc. Natl. Acad. Sci. USA *112*, 11941–11946.

Ridlon, J.M., Harris, S.C., Bhowmik, S., Kang, D.-J., and Hylemon, P.B. (2016). Consequences of bile salt biotransformations by intestinal bacteria. Gut Microbes *7*, 22–39.

Riley, A.B., Kim, D., and Hansen, A.K. (2017). Genome sequence of "*Candidatus* Carsonella ruddii" strain BC, a nutritional endosymbiont of *Bactericera cockerelli*. Genome Announc. *5*, e00236–17.

Roberts, J.W., Roberts, C.W., and Craig, N.L. (1978). *Escherichia coli recA* gene product inactivates phage lambda repressor. Proc. Natl. Acad. Sci. USA *75*, 4714–4718.

Rone, M.B., Midzak, A.S., Issop, L., Rammouz, G., Jagannathan, S., Fan, J., Ye, X., Blonder, J., Veenstra, T., and Papadopoulos, V. (2012). Identification of a dynamic mitochondrial protein complex driving cholesterol import, trafficking, and metabolism to steroid hormones. Mol. Endocrinol. *26*, 1868–1882.

Roux, S., Enault, F., Hurwitz, B.L., and Sullivan, M.B. (2015). VirSorter: mining viral signal from microbial genomic data. PeerJ *3*, e985.

Salyers, A.A., Bonheyo, G., and Shoemaker, N.B. (2000). Starting a new genetic system: lessons from *Bacteroides*. Methods *20*, 35–46.

Salyers, A.A., Vercellotti, J.R., West, S.E., and Wilkins, T.D. (1977). Fermentation of mucin and plant polysaccharides by strains of *Bacteroides* from the human colon. Appl. Environ. Microbiol. *33*, 319–322.

Schmidt, T.S.B., Raes, J., and Bork, P. (2018). The human gut microbiome: from association to modulation. Cell *172*, 1198–1215.

Seguritan, V., Jr., Alves, N., Jr., Arnoult, M., Raymond, A., Lorimer, D., Burgin, A.B., Jr., Salamon, P., and Segall, A.M. (2012). Artificial neural networks trained to detect viral and phage structural proteins. PLoS Comput. Biol. *8*, e1002657.

Sekulovic, O., and Fortier, L.-C. (2015). Global transcriptional response of Clostridium difficile carrying the CD38 prophage. Appl. Environ. Microbiol. *81*, 1364–1374.

Shen, Y., Giardino Torchia, M.L., Lawson, G.W., Karp, C.L., Ashwell, J.D., and Mazmanian, S.K. (2012). Outer membrane vesicles of a human commensal mediate immune regulation and disease protection. Cell Host Microbe *12*, 509–520.

Shkoporov, A.N., Khokhlova, E.V., Fitzgerald, C.B., Stockdale, S.R., Draper, L.A., Ross, R.P., and Hill, C. (2018). ΦCrAss001 represents the most abundant bacteriophage family in the human gut and infects *Bacteroides intestinalis*. Nat. Commun. *9*, 4781.

Shoemaker, N.B., Vlamakis, H., Hayes, K., and Salyers, A.A. (2001). Evidence for extensive resistance gene transfer among *Bacteroides* spp. and among *Bacteroides* and other genera in the human colon. Appl. Environ. Microbiol. *67*, 561–568.

Simon, R., Priefer, U., and Pühler, A. (1983). A broad host range mobilization system for *in vivo* genetic engineering: transposon mutagenesis in Gram negative bacteria. Nat. Biotechnol. *1*, 784–791.

Sullivan, M.B., Coleman, M.L., Weigele, P., Rohwer, F., and Chisholm, S.W. (2005). Three *Prochlorococcus* cyanophage genomes: signature features and ecological interpretations. PLoS Biol. *3*, e144.

Tartera, C., and Jofre, J. (1987). Bacteriophages active against *Bacteroides fragilis* in sewage-polluted waters. Appl. Environ. Microbiol. *53*, 1632–1637.

Tatusov, R.L., Fedorova, N.D., Jackson, J.D., Jacobs, A.R., Kiryutin, B., Koonin, E.V., Krylov, D.M., Mazumder, R., Mekhedov, S.L., Nikolskaya, A.N., et al. (2003). The COG database: an updated version includes eukaryotes. BMC Bioinformatics *4*, 41.

Thornton, R.F., Murphy, E.C., Kagawa, T.F., O'Toole, P.W., and Cooney, J.C. (2012). The effect of environmental conditions on expression of *Bacteroides fragilis* and *Bacteroides thetaiotaomicron* C10 protease genes. BMC Microbiol. *12*, 190.

Tuncil, Y.E., Xiao, Y., Porter, N.T., Reuhs, B.L., Martens, E.C., and Hamaker, B.R. (2017). Reciprocal prioritization to dietary glycans by gut bacteria in a competitive environment promotes stable coexistence. MBio *8*, e01068–17.

Whittle, G., Hund, B.D., Shoemaker, N.B., and Salyers, A.A. (2001). Characterization of the 13-kilobase *ermF* region of the *Bacteroides* conjugative transposon CTnDOT. Appl. Environ. Microbiol. *67*, 3488–3495.

Winter, S.E., Thiennimitr, P., Winter, M.G., Butler, B.P., Huseby, D.L., Crawford, R.W., Russell, J.M., Bevins, C.L., Adams, L.G., Tsolis, R.M., et al. (2010). Gut inflammation provides a respiratory electron acceptor for *Salmonella*. Nature *467*, 426–429.

Yao, L., Seaton, S.C., Ndousse-Fetter, S., Adhikari, A.A., DiBenedetto, N., Mina, A.I., Banks, A.S., Bry, L., and Devlin, A.S. (2018). A selective gut bacterial bile salt hydrolase alters host metabolism. eLife *7*, e37182.

Yeliseev, A.A., and Kaplan, S. (1999). A novel mechanism for the regulation of photosynthesis gene expression by the TspO outer membrane protein of *Rhodobacter sphaeroides* 2.4.1. J. Biol. Chem. *274*, 21234–21243.

Young, R. (2014). Phage lysis: three steps, three choices, one outcome. J. Microbiol. *52*, 243–258.

Yu, C.S., Cheng, C.W., Su, W.C., Chang, K.C., Huang, S.W., Hwang, J.K., and Lu, C.H. (2014). CELLO2GO: a web server for protein subCELlular LOcalization prediction with functional gene ontology annotation. PLoS ONE *9*, e99368.

Yutin, N., Makarova, K.S., Gussow, A.B., Krupovic, M., Segall, A., Edwards, R.A., and Koonin, E.V. (2018). Discovery of an expansive bacteriophage family that includes the most abundant viruses from the human gut. Nat. Microbiol. *3*, 38–46.

Zeno, S., Veenman, L., Katz, Y., Bode, J., Gavish, M., and Zaaroor, M. (2012). The 18 kDa mitochondrial translocator protein (TSPO) prevents accumulation of protoporphyrin IX. Involvement of reactive oxygen species (ROS). Curr. Mol. Med. *12*, 494–501.

Zhao, S., Lieberman, T.D., Poyet, M., Kauffman, K.M., Gibbons, S.M., Groussin, M., Xavier, R.J., and Alm, E.J. (2019). Adaptive evolution within gut microbiomes of healthy people. Cell Host Microbe *25*, 656–667.e8.

STAR★METHODS

KEY RESOURCES TABLE

REAGENT or RESOURCE	SOURCE	IDENTIFIER
Bacterial and Virus Strains		
Bacteroides vulgatus ATCC 8482	ATCC	ATCC 8482
B. vulgatus Δ*tdk*	This paper	N/A
B. vulgatus Δ*int*	This paper	N/A
B. vulgatus ΔBV01	This paper	N/A
B. vulgatus ΔBV01Δ*tspO*	This paper	N/A
B. vulgatus ΔBV01, *attN*::pNBU2-*bla-ermGb*	This paper	N/A
B. vulgatus BV01-*tetQ, attN::pNBU2-bla-cfx*	This paper	N/A
B. vulgatus ΔBV01, *attB*::BV01-*tetQ, attN*::pNBU2-*bla-ermGb*	This paper	N/A
B. vulgatus VPI-4245	Abigail Salyers	N/A
B. vulgatus VPI-2365	Abigail Salyers	N/A
B. vulgatus VPI-6186	Abigail Salyers	N/A
B. vulgatus VPI-5710	Abigail Salyers	N/A
B. vulgatus DH4096S	Abigail Salyers	N/A
B. ovatus ATCC 8483	ATCC	ATCC 8483
Chemicals, Peptides, and Recombinant Proteins		
Taurocholic acid sodium salt hydrate, ≥ 95%	Sigma-Aldrich	CAS #345909-26-4
Glycocholic acid hydrate, ≥ 97%	Sigma-Aldrich	CAS #1192657-83-2
Critical Commercial Assays		
Nextera XT Library Preparation Kit	Illumina	Cat. #FC-131-1096
Nextera XT Index Kit	Illumina	Cat. #FC-131-1002
NEBNext Ultra II FS Kit for Illumina	New England Biolabs	E7805L
RNeasy Kit	QIAGEN	Cat. #74104
Deposited Data		
Mutant genome DNA sequencing, see Table S3	This paper	PRJNA655911
RNA sequencing, see Table S3	This paper	PRJNA622597
Wastewater virome DNA sequencing, see Table S3	This paper	PRJNA622299
Bacterial genomes, see Table S3	This paper	PRJNA622758
Phage DNA sequencing, see Table S3	This paper	PRJNA655697
Experimental Models: Organisms/Strains		
Germfree C57BL/6J mice	UCR Gnotobiotic Facility	N/A
Oligonucleotides		
Primers for strain construction, see Table S4	This paper	N/A
Primers for integrase activity assays, see Table S4	This paper	N/A
Primers for detection of *Salyersviridae* phages, see Table S4	This paper	N/A
Recombinant DNA		
pKNOCK-*bla-ermG*$_b$	Koropatkin et al., 2008	N/A
pExchange-*tdk*BV	This paper	N/A
pNBU2-*bla-ermG*$_b$	Koropatkin et al., 2008	N/A
pNBU2-*int*	This paper	N/A
pNBU2-*bla-cfx*	This paper	N/A

(*Continued on next page*)

Continued

REAGENT or RESOURCE	SOURCE	IDENTIFIER
Software and Algorithms		
Breseq	Deatherage and Barrick, 2014	https://github.com/barricklab/breseq
A5ud	Riley et al., 2017	https://github.com/phdegnan/A5ud
bwa	Li and Durbin, 2009	https://github.com/lh3/bwa
Microbialomics	This paper	https://github.com/phdegnan/MICROBIALOMICS
Rockhopper	McClure et al., 2013	https://cs.wellesley.edu/~btjaden/Rockhopper/
Trimmomatic 0.38	Bolger et al., 2014	http://www.usadellab.org/cms/?page=trimmomatic
metaSPAdes v3.13.0	Nurk et al., 2017	https://github.com/ablab/spades
Other		
30,000 MWCO Corning Spin-X UF 20 Concentrators	Sigma-Aldrich	Cat. #CLS431489
Vivaflow 50R 30,000 MWCO Hydrosart Filter	Sartorius	Cat. #VF05H2
Sep-Pak tC18 500 mg cartridges	Waters Corp	Cat. #WAT036790

RESOURCE AVAILABILITY

Lead Contact

Further information and requests for resources and reagents should be directed to and will be fulfilled by the Lead Contact, Dr. Patrick Degnan (patrick.degnan@ucr.edu).

Materials Availability

Bacterial strains and plasmids generated in this study are available upon request to the Lead Contact, Dr. Patrick Degnan (patrick.degnan@ucr.edu).

Data and Code Availability

Trimmed DNA sequencing reads from mutant genomes generated in this study are deposited in the NCBI SRA under PRJNA655911. Trimmed RNA sequencing reads from this study are deposited in the NCBI SRA under PRJNA622597. Trimmed wastewater virome DNA sequencing reads are deposited in the NCBI SRA under PRJNA622299. Ten new assembled *B. vulgatus* genomes are deposited in NCBI GenBank under PRJNA622758. Untrimmed phage DNA sequencing reads from culture supernatants are deposited in the NCBI SRA under PRJNA655697. All NCBI BioSample Accession numbers are listed in Table S3. The code for annotation of bacterial genomes is available at https://github.com/phdegnan/MICROBIALOMICS.

EXPERIMENTAL MODEL AND SUBJECT DETAILS

Bacterial Strains

A list of bacterial strains used in this work can be found in the Key Resources Table and Table S4. *Escherichia coli* S17-1 λ *pir* was grown aerobically in Lysogeny Broth (LB; 10 g/L tryptone, 5 g/L yeast extract, 5 g/L NaCl) at 37°C under agitation. *Bacteroides* strains were cultured anaerobically in a vinyl anaerobic chamber using 70% N_2, 20% CO_2, and 10% H_2 gas mixture (Coy Laboratory Products, Grass Lake, MI). All *Bacteroides* cultures were grown on Difco Brain Heart Infusion (BHI) agar supplemented with 10% defibrinated horse blood (BHI-HB; Quad Five, Ryegate, MT), or in tryptone-yeast extract-glucose broth (TYG; 10 g/L tryptone, 5 g/L yeast extract, 2 g/L glucose, 500 mg/L cysteine free base, 100 mM pH 7.2 potassium phosphate, 20 mg/L $MgSO_4 \cdot 7H_2O$, 400 mg/L $NaHCO_3$, 80 mg/L NaCl, 100 mg/L resazurin, 0.0008% $CaCl_2$, 0.4 μg/L $FeSO_4$, 1 μg/L menadione, 0.2 mM histidine, 1.9 μM hematin) at 37°C. When necessary, ampicillin (100 μg/mL), gentamicin (200 μg/mL), erythromycin (25 μg/mL), 5′-flourodeoxyuridine (FUdR; 20 μg/mL), or tetracycline (2 μg/mL) were supplemented in the media.

Mice

Germfree C57BL/6J mice were used in this study. With no *a priori* reason to expect age to influence transduction rates, animals ranged from 7 weeks to nearly 12 months old. Animals were maintained in flexible plastic gnotobiotic isolators with a 12-hr light/dark cycle. Animals caged individually (n = 1, female) or in pairs of litter mates (n = 6, males) were provided with standard, autoclaved mouse chow (5K67 LabDiet, Purina) *ad libitum*. All experiments using mice were performed using protocols approved by the University of California Riverside Institutional Animal Care and Use Committee.

METHOD DETAILS

Cloning and Mutagenesis

All primers used to construct genetic mutants are listed in Table S4. Markerless deletion mutants in *B. vulgatus* were achieved by allelic exchange using a system analogous to that developed in *B. thetaiotaomicron,* (Koropatkin et al., 2008) and confirmed by PCR and whole genome sequencing. The *tdk* gene (BVU_RS09305), encoding thymidine kinase, was deleted from *B. vulgatus* ATCC 8482 by allelic exchange, conferring resistance to the toxic nucleotide analog FUdR. Cloning was performed as described by (Degnan et al., 2014). Briefly, the 3.5 Kb regions flanking either side of *tdk* were amplified with Kapa HiFi Taq MasterMix (Kapa Biosystems, Wilmington, MA) and joined by splicing overlap exchange (SOE) PCR. The SOE product was purified, restriction digested, and ligated into the suicide vector pKNOCK-*bla*-*ermG*$_b$ in *E. coli*, and conjugated into *B. vulgatus.* Single recombinant merodiploids were selected for on BHI-HB supplemented with gentamicin and erythromycin, and double recombinant deletion mutants subsequently selected for on BHI-HB with FUdR. The counterselectable suicide vector pExchange-*tdk*BV was constructed by amplifying *tdk* from *B. vulgatus* and cloning the *tdk* amplicon into pKNOCK-*bla*-*ermG*$_b$ by the same methods used to clone the SOE product above.

Subsequent deletions were accomplished similarly as described for *tdk*, except using pExchange-*tdk*BV and flanking regions of ~1 Kb to create the deletion alleles (*tspO, int*). For deletion of the entire BV01 prophage, an empty attachment site (*attB*) and the flanking 800 bp were cloned from *B. vulgatus* VPI-4506, which is 99.9% nucleotide identical to the analogous regions flanking BV01 in *B. vulgatus* ATCC 8482.

Complementation of the BV01 integrase (BVU_RS14130) was accomplished by cloning the gene and its native promoter into the integrative plasmid pNBU2-*bla*-*ermG*b, which has a single integration site in the *B. vulgatus* genome (*attN*; RefSeq: NC_009614.1; 2,710,334-2,710,346). This construct was conjugated into *B. vulgatus* and transconjugants selected for on BHI-HB supplemented with gentamicin and erythromycin (Degnan et al., 2014).

The BV01-*tetQ* strain was constructed by inserting *tetQ* from pNBU2-*bla*-*tetQ* immediately downstream of the stop codon of BVU_RS14265, upstream of a predicted transcriptional terminator. As was done for deletion constructs, the desired region was constructed on the pExchange-*tdk*BV plasmid and moved into the wild-type *B. vulgatus* strain by allelic exchange. First, a ~2 Kb region surrounding the BVU_RS14265 stop codon was amplified in two pieces with SOE primers designed to insert adjacent SpeI and BamHI cut sites downstream of the stop codon and ligated into pExchange-*tdk*BV. This construct was confirmed by Sanger sequencing before *tetQ* and its promoter were amplified from CTnDOT, and ligated into the SpeI and BamHI cut sites. Tetracycline was used to select for mutants, and release of BV01-*tetQ* phages confirmed by PCR.

Select mutant strains were confirmed by whole genome sequencing and analyzed with Breseq (Deatherage and Barrick, 2014) aligned to the wild-type *B. vulgatus* ATCC 8482 genome (RefSeq: NC_009614.1), and summarized in Table S2.

Bacterial Growth Rate

Triplicate 200 μL cultures of *B. vulgatus* strains were grown in TYG medium and their optical densities (OD) monitored at a wavelength of 600 nm at 30 min intervals. Doubling times were calculated from cells in early to mid-log phase using the least-squares fitting method on http://www.doubling-time.com/compute.php.

Genome Sequencing

Cells were pelleted from 5 mL overnight culture in TYG by centrifugation at 4,000 × *g* for 5 min at 4°C, resuspended in 0.5 mL TE buffer (10 mM Tris, 1 mM EDTA), and lysed by adding sodium dodecyl sulfate (SDS) and proteinase K (GoldBio, Olivette, MO) to final concentrations of 0.07% and 300 μg/mL, respectively, and incubating for 2 hr at 55°C. Cellular material was removed by washing twice in an equal volume of buffered phenol, phenol-chloroform-isoamyl alcohol (VWR, Radnor, PA), and DNA precipitated with 100% ethanol in the presence of 0.3M sodium acetate at −20°C overnight. DNA pellets were washed with 70% ethanol, dried, and resuspended in TE buffer.

Phage DNA was prepared from overnight TYG culture supernatants collected after centrifugation and filtration with a 0.22 μm filter and concentrated by centrifugation with 30,000 MWCO Corning Spin-X UF 20 Concentrators (Corning, NY) or by tangential flow filtration with a Vivaflow 50R 30,000 MWCO Hydrosart filter (Sartorius, Gottingen, Germany). Supernatants were treated with 200 μg/mL DNase I and 1 μg/mL RNase A for 1 hr at room temperature to remove unprotected DNA and RNA. Virions were disrupted with 1% SDS and 1 mg/mL proteinase K for 2 hr at 55°C. DNA was further isolated using the same phenol-chloroform-isoamyl alcohol extraction and ethanol precipitation procedures as for cellular DNA.

DNA libraries were constructed with the Nextera XT Library Preparation Kit and Index Kit (Illumina, San Diego, CA) or the NEBNext Ultra II FS kit for Illumina (New England Biolabs, Ipswich, MA). DNA libraries were pooled and sequenced on an Illumina HiSeq5000, HiSeq2500 and MiSeq instruments. Fastq files were generated from demultiplexed reads with bcl2fastq Conversion Software (Illumina, San Diego, CA). Reads were trimmed and assembled using the A5ud pipeline (Riley et al., 2017). Sequencing methods and assembly data are summarized in Table S3. Reads were mapped to the *B. vulgatus* ATCC 8482 reference genome (RefSeq: NC_009614.1) using bwa in paired end mode (Li and Durbin, 2009) with default parameters to generate Figure 1A.

Genome Annotation

Annotation of cellular genomes was accomplished with a custom Perl script (https://github.com/phdegnan/MICROBIALOMICS) that calls protein coding genes with Prodigal (Hyatt et al., 2010) and RNA coding genes with tRNAscan-SE (Lowe and Eddy, 1997), Rnammer (Lagesen et al., 2007) and Infernal (Nawrocki and Eddy, 2013). Functional predictions are assigned by searching against Kyoto Encyclopedia of Genes and Genomes (Kanehisa and Goto, 2000), Cluster of Orthologous Genes (Tatusov et al., 2003), Pfam (Bateman et al., 2004), and TIGRFAM (Haft et al., 2003) databases, and subCELlular LOcalization predictor (Yu et al., 2014) is used to predict cellular localization.

For phage genomes, open reading frames were called by Prodigal and the gene calling tool within Artemis (Carver et al., 2012). Functional predictions were made as above except with relaxed search parameters (cut_nc in hmmscan), plus using Basic Local Search Alignment Tool (Mount, 2007) with the GenBank virus database (Benson et al., 2009), Phyre2 (Kelley et al., 2015) to identify conserved protein folds, SignalP 5.0 (Almagro Armenteros et al., 2019) to predict signal peptides, and iVireons (Seguritan et al., 2012) to predict structural proteins, and manually comparing and combining results.

In Vivo Transduction

Individually antibiotic resistance marked bacterial strains were grown for ~20h in TYG medium with appropriate antibiotics and frozen at −80°C in anaerobic cryovials. Cell viability was tested by plating and viable CFU counts were used to combine equal parts of the *B. vulgatus* cured lysogen tagged with pNBU2-*bla-ermGb* and *B. vulgatus* BV01-*tetQ* tagged with pNBU2-*bla-cfx*. Approximately 4×10^6 CFUs of the combined strains were administered to each animal by oral gavage. Fecal samples were collected on days 1, 3, 7 and 11 from each animal. Fecal pellets were processed by adding 500μl of TYG+20% glycerol to each tube and vigorously shaking in a beadbeater without beads for 1 m 30 s. Fecal slurries were spun down at 2,000 x g for 1 s, followed by serial dilution on selective media (BHI+Tet+Gn, BHI+Erm+Gn, BHI+Erm+Tet+Gn) to determine CFUs. Animals were sacrificed on day 11 following final fecal collection.

Integrase Activity Assays

Integrase activity was assayed through PCR of DNase-treated supernatant DNA. Briefly, free phage DNA was prepared as for DNA sequencing, and amplified with Kapa HiFi Taq MasterMix with primers specific to BV01 (BVU_RS14350) or spanning the circularized *attP* (Table S4). Free phage DNAs were checked for the presence of contaminating cellular DNA by amplifying the 16S rRNA gene with universal primers. Amplicons were cleaned with a QIAGEN PCR Cleanup kit (Hilden, Germany) and run on an agarose gel in 0.5X Tris-borate-EDTA buffer at 70V alongside 1 Kb ladder (New England BioLabs, Ipswich, MA) or GeneRuler Express DNA Ladder (Thermo Scientific, Waltham, MA) and stained with GelRed (VWR, Radnor, PA). Amplicons generated with *attP*-flanking primers were sequence confirmed by Sanger sequencing performed by ACGT, Inc (Wheeling, IL).

Transcriptomics

B. vulgatus was grown overnight in 5 mL TYG medium. Each culture was pelleted (4,000 × *g* for 5 min at 4°C), supernatant decanted, and washed in an equal volume of TYG three times. Cells were normalized to an OD_{600} of ~0.3 (~2.9×10^9 CFU/mL) and used to inoculate cultures in 10 mL TYG at a final dilution of 1:1000 in biological triplicate. Cell growth was monitored and cells were harvested at an OD_{600} of ~0.4 (3.9×10^9 CFU/mL). Total RNA was prepared with a QIAGEN RNeasy kit (Hilden, Germany) and treated on-column with RNase-free DNase (QIAGEN, Hilden, Germany). RNA was quantitated with a Qubit 2.0 fluorometer (Thermo Fisher, Waltham, MA) and stored at −80°C.

RNA was submitted to the W. M. Keck Center for Comparative and Functional Genomics at the University of Illinois at Urbana-Champaign for quality analysis, rRNA depletion with the RiboZero Bacteria kit (Illumina, San Diego, CA), library construction with the TruSeq Stranded mRNAseq Sample Prep kit (Illumina, San Diego, CA), and sequencing on an Illumina NovaSeq 6000 with the NovaSeq S4 reagent kit. Fastq files of demultiplexed reads were prepared with the bcl2fastq v2.20 Conversion Software (Illumina, San Diego, CA).

RNaseq reads were quality filtered and trimmed with trim_galore v0.4.4 (https://www.bioinformatics.babraham.ac.uk/projects/trim_galore/). Rockhopper (McClure et al., 2013) was used to calculate individual transcript Expression and pairwise *q*-values. Fold-change was calculated in Excel as (Expression A)/(Expression B) if A > B, or as –(Expression B)/(Expression A) if B > A. Differentially expressed transcripts between the isogenic mutants were defined as those ≥ 2-fold change and $q \leq 0.01$. Trimmed reads were mapped to the *B. vulgatus* ATCC 8482 reference genome (RefSeq: NC_009614.1) using bwa in single end mode (Li and Durbin, 2009) with default parameters to generate coverage curves.

Bile Salt Deconjugation Assay and LC-MS

B. vulgatus strains were inoculated in TYG liquid supplemented with 50 μM glycocholic acid (GCA) or 50 μM taurocholic acid (TCA) and allowed to grow for 16 or 48 hr, respectively. *B. vulgatus* ATCC 8482 had previously been shown to completely hydrolyze TCA in 48 hr (Yao et al., 2018); the 16 hr time point was chosen to ensure incomplete hydrolysis to better detect increased activity. *B. vulgatus* ATCC 8482 was also unable to hydrolyze GCA in 48 hr (Yao et al., 2018); the 48 hr time point was chosen to ensure that any increase in hydrolysis would be apparent. Grown cultures were brought to a pH 2.0-3.0 with 10 N hydrochloric acid, centrifuged for 5 min at 4,000 x *g*, and the pellets discarded. Bile acids were isolated by solid phase extraction over Sep-Pak

tC18 500 mg cartridges (Waters Corp., Milford, MA). Cartridges were preconditioned by serial washes with 6 mL hexane, 3 mL acetone, 6 mL methanol, and 6 mL water (pH = 3.0). Acidified supernatants were loaded before washing with 3 mL 40% methanol. The column was allowed to dry, then bile acids eluted in 3 mL methanol. Samples were evaporated under nitrogen, resuspended in 20 μL methanol, and centrifuged before analysis by liquid chromatography-mass spectroscopy (LC-MS).

LC-MS for all samples was performed on a Waters Aquity UPLC coupled with a Waters Synapt G2-Si ESI MS. Chromatography was performed using a Waters Cortecs UPLC C18 column (1.6 μm particle size) (2.5 mm x 50 mm) with a column temperature of 40°C. Samples were injected at 1 μl. Solvent A consisted of 95% water, 5% acetonitrile, and 0.1% formic acid. Solvent B consisted of 95% acetonitrile, 5% water, and 0.1% formic acid. The initial mobile phase was 90% Solvent A, 10% Solvent B and increased linearly until the gradient reached 50% Solvent A and 50% Solvent B at 7.5 min. Solvent B was increased linearly again until it was briefly 100% at 8.0 min until returning to the initial mobile phase (90% Solvent A, 10% Solvent B) over the next 2 min. The total run was 10 min with a flow rate of 10 μL/min. MS was performed in negative ion mode. Nebulizer gas pressure was maintained at 400°C and gas flow was 800 L/hour. The capillary voltage was set at 2,000 V in negative mode. MassLynx was used to visualize and analyze chromatographs, including calculating areas under the curve (AUC). Ratios of AUCs are presented in Figure 5C.

Taxonomic nomenclature

The family, subfamily, and generic viral taxa names were chosen to honor the microbiologist Abigail A. Salyers, who made significant contributions to understanding the functions and genetics of human gut anaerobes and the importance of their mobile genetic elements.

Wastewater collection, processing, and viromics

From the Urbana and Champaign Sanitary District Northeast Plant (Urbana, IL), 1 L of unprocessed wastewater was collected at each of three time points: May 25, 2016, June 23, 2016, and October 3, 2016.

Wastewater samples were transported on ice, immediately centrifuged at 2,500 × *g* for 10 min at 4°C and filtered through a 0.4 μm polyethersulfone filter to remove large particulate and cellular matter. The sample was split into three aliquots and processed three ways. One aliquot was not processed further (F). Another aliquot was filtered a second time through a 0.22 μm polyethersulfone filter (DF). The last aliquot was washed three times with an equal volume of chloroform (FC). All aliquots were concentrated 100-fold and virome DNA was isolated from each as described for genome sequencing of phages.

DNA libraries of virome DNA were prepared using the same methods as described for phage genome sequencing and were sequenced on an Illumina HiSeq 2500 sequencer with a HiSeq v4 SBS sequencing kit (Illumina, San Diego, CA) producing 2 × 160-bp paired-end reads. Fastq files of demultiplexed reads were generated with the bcl2fastq v2.17.1.14 Conversion Software (Illumina, San Diego, CA). Reads were trimmed and quality filtered using Trimmomatic 0.38 (Bolger et al., 2014) and assembled with metaSPAdes v3.13.0 using default parameters (Nurk et al., 2017). Sequencing and assembly data for wastewater viromes is summarized in Table S4. Read mapping to phage genomes was performed with bwa in paired end mode (Li and Durbin, 2009).

Human Microbiome Project Healthy Human Subjects Study samples were downloaded with portal_client (Table S6). Read mapping was performed with bwa (Li and Durbin, 2009).

QUANTIFICATION AND STATISTICAL ANALYSIS

Statistical tests, number of events quantified, standard deviation of the mean, and statistical significance is reported in figure legends. ANOVA and Tukey HSD tests were run on http://vassarstats.net/anova1u.html.

Cell Reports, Volume *32*

Supplemental Information

Infection with Bacteroides Phage BV01 Alters the Host Transcriptome and Bile Acid Metabolism in a Common Human Gut Microbe

Danielle E. Campbell, Lindsey K. Ly, Jason M. Ridlon, Ansel Hsiao, Rachel J. Whitaker, and Patrick H. Degnan

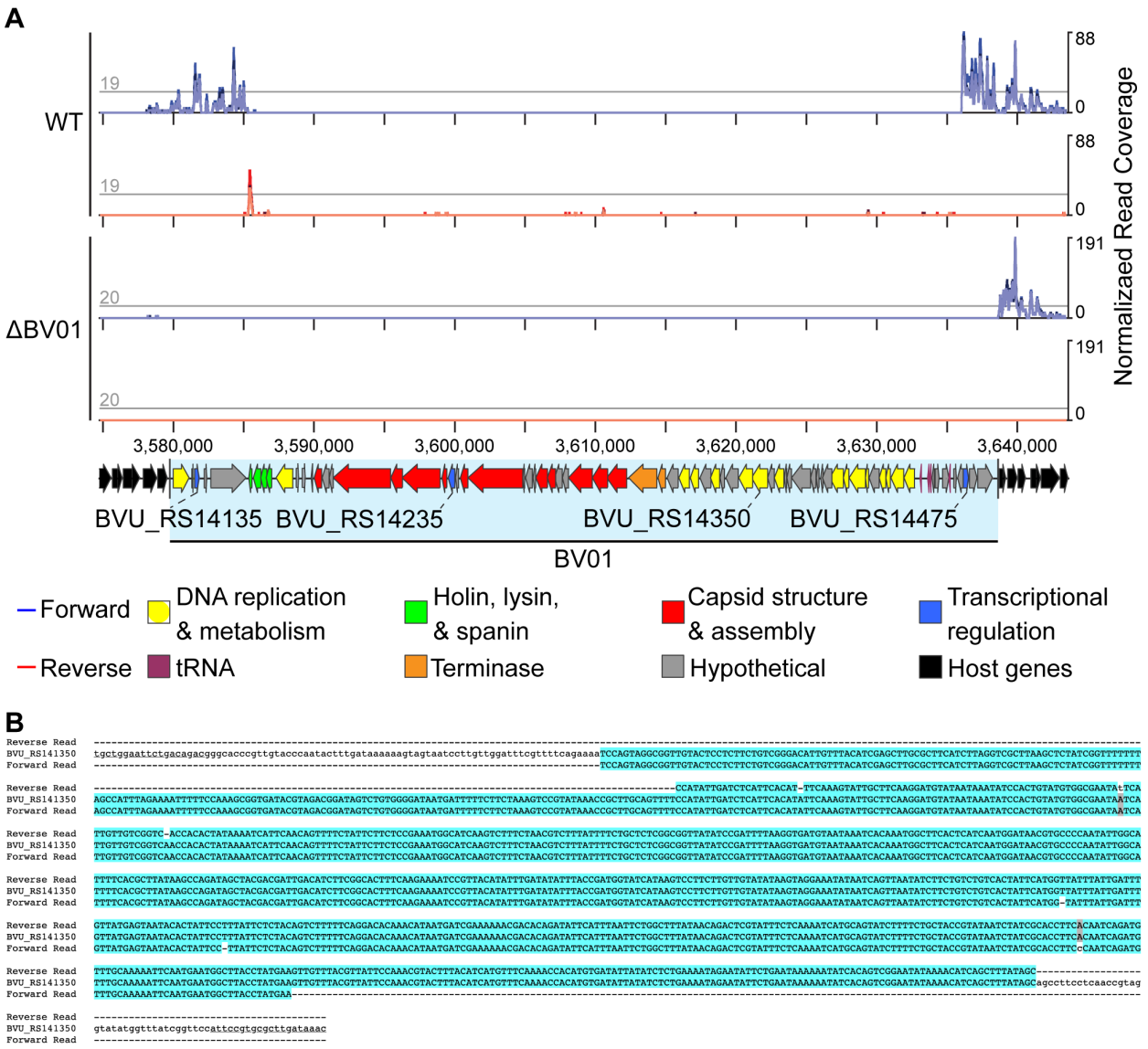

Figure S1. Transcriptional activity at BV01 attachment site and confirmation of free BV01 integrase amplicons.
Related to Figures 1, 2, and 3. (A) RNAseq reads from wild-type lysogen (WT) and cured lysogen (ΔBV01) strains were mapped to the region, and coverage was normalized to the total number of reads mapping to the genome. Locations of the phage marker gene (BVU_RS14350) and three phage transcriptional regulators are indicated: the putative phage repressor (BVU_RS14475), anti-repressor (BVU_RS14135), and an RNA polymerase sigma factor (BVU_RS14235). Three replicates shown. The average normalized read coverage for each genome is displayed as the grey line. Maximum read coverage for the region is indicated on the y-axis. Forward transcription (red) and reverse transcription (blue) were plotted separately. (B) Nucleotide alignment of BVU_RS14350 with trimmed Sanger sequencing data generated from DNase-treated cell-free BV01 supernatant. Despite appearing larger in size by gel electrophoresis (Fig. 2B), no large insertions were detected. Locations of primers used to amplify BVU_RS14350 and for Sanger sequencing denoted by underlined sequence.

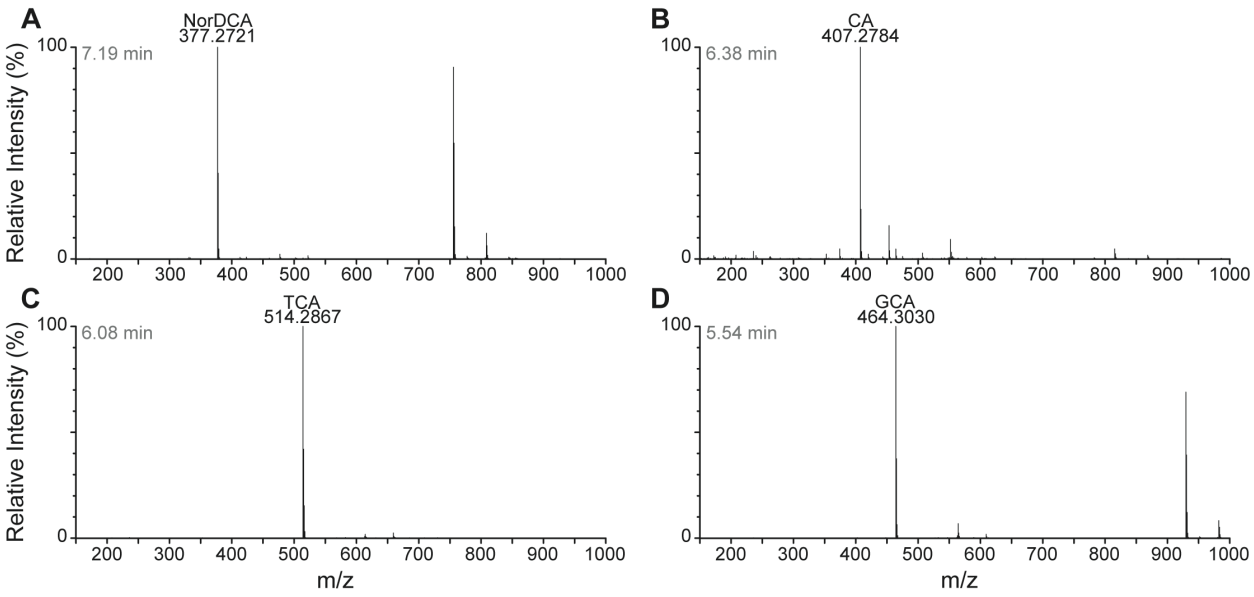

Figure S2. Representative extracted ion count (EIC) chromatograms for the bile acid species of interest. Related to Figure 5. EIC are shown for (A) the internal control nordeoxycholic acid (NorDCA), (B) the product of bile acid deconjugation, cholic acid (CA), taurocholic acid (TCA), and glycocholic acid (GCA). Times of flight indicated in grey.

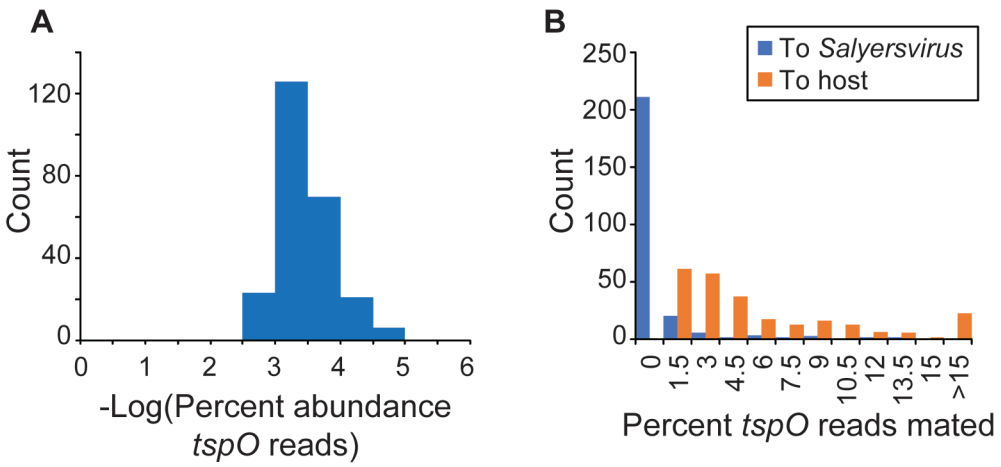

Figure S3. Prevalence of prophage insertion adjacent to *tspO* in human gut samples. Related to Figures 4 and 6. Reads from 246 healthy human gut metagenomes were obtained from the Human Microbiome Project Healthy Human Subjects Study. (A) Reads were first mapped to representative sequences of *tspO* from *B. vulgatus* and *B. dorei*. Percent abundance *tspO* reads was calculated on a per sample basis as the number of reads mapping to *tspO* divided by the total number of reads. Histogram shows counts of samples. (B) Reads mapping to *tspO* were filtered to only include reads antisense to *tspO*, predicted to point toward the *attB* based on the known genomic architecture. Mates to those reads were subsequently mapped to either the empty *B. vulgatus attB* (To host) or to BV01 and its *Salyersvirus* relatives (To *Salyersvirus*) (Fig. 6). Percent *tspO* reads mated was calculated as the read pairs bridging *tspO* and the sequence of interest, sequence divided by the total number of reads mapping antisense to *tspO*. Histogram shows counts of samples.

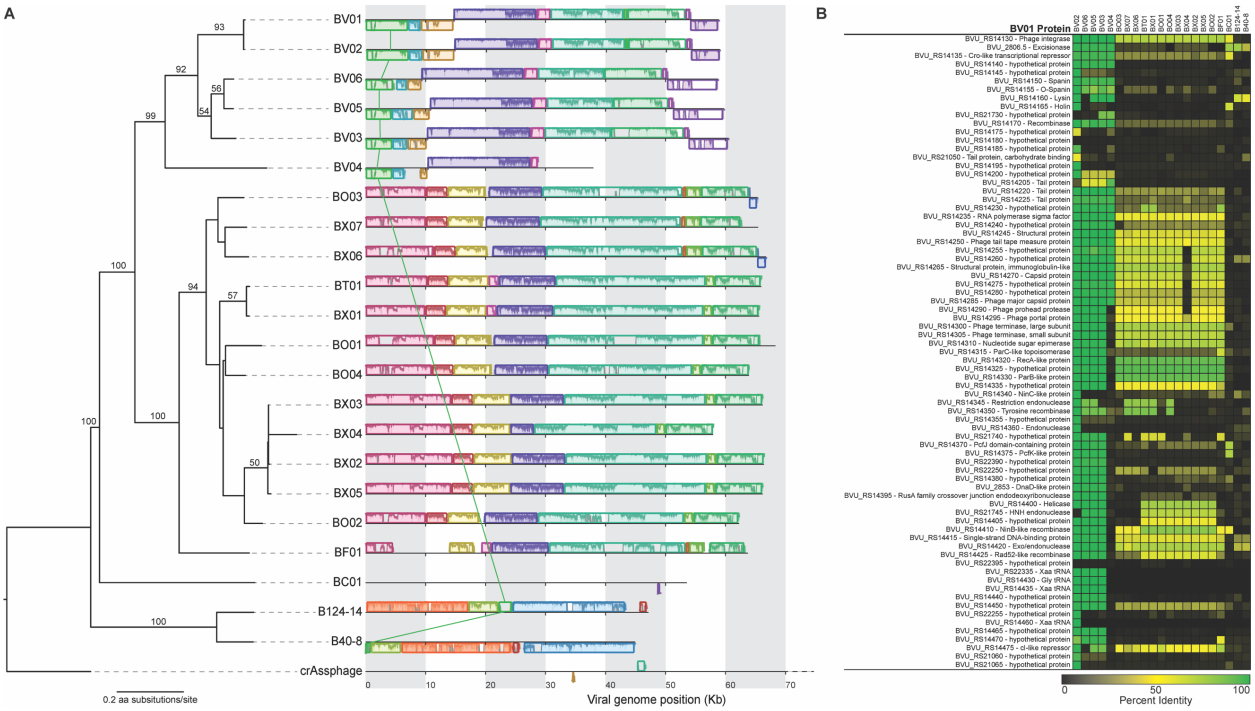

Figure S4. Whole genome tree, nucleotide alignment and proteomic similarity of *Salyersviridae* phages. Related to Figure 6. (A) Phylogenomic Genome-BLAST Distance Phylogeny implemented with the VCTOR online tool (Meier-Kolthoff and Göker, 2017) using amino acid data from all phage ORFs. For consistency, all phage genomes were annotated with MetaGeneAnnotator (Noguchi et al., 2008) implemented via VirSorter (Roux et al., 2015). Support values above branches are GBDP pseudo-bootstrap values from 100 replications. Genome alignment of all phages made with MAUVE. One locally collinear block (LCB) connects phages B124-14 and B40-8 to the *Salyersviridae* at the nucleotide level (green). Other LCB connecting lines removed for clarity. (B) Gene similarity matrix for BV01-encoded genes among the S*alyersviridae*. Genes for non-BV01 predicted phages were predicted with Prodigal (Hyatt et al., 2010). Similarity was computed as amino acid percent identity for protein coding genes and nucleotide percent identity for tRNA genes.

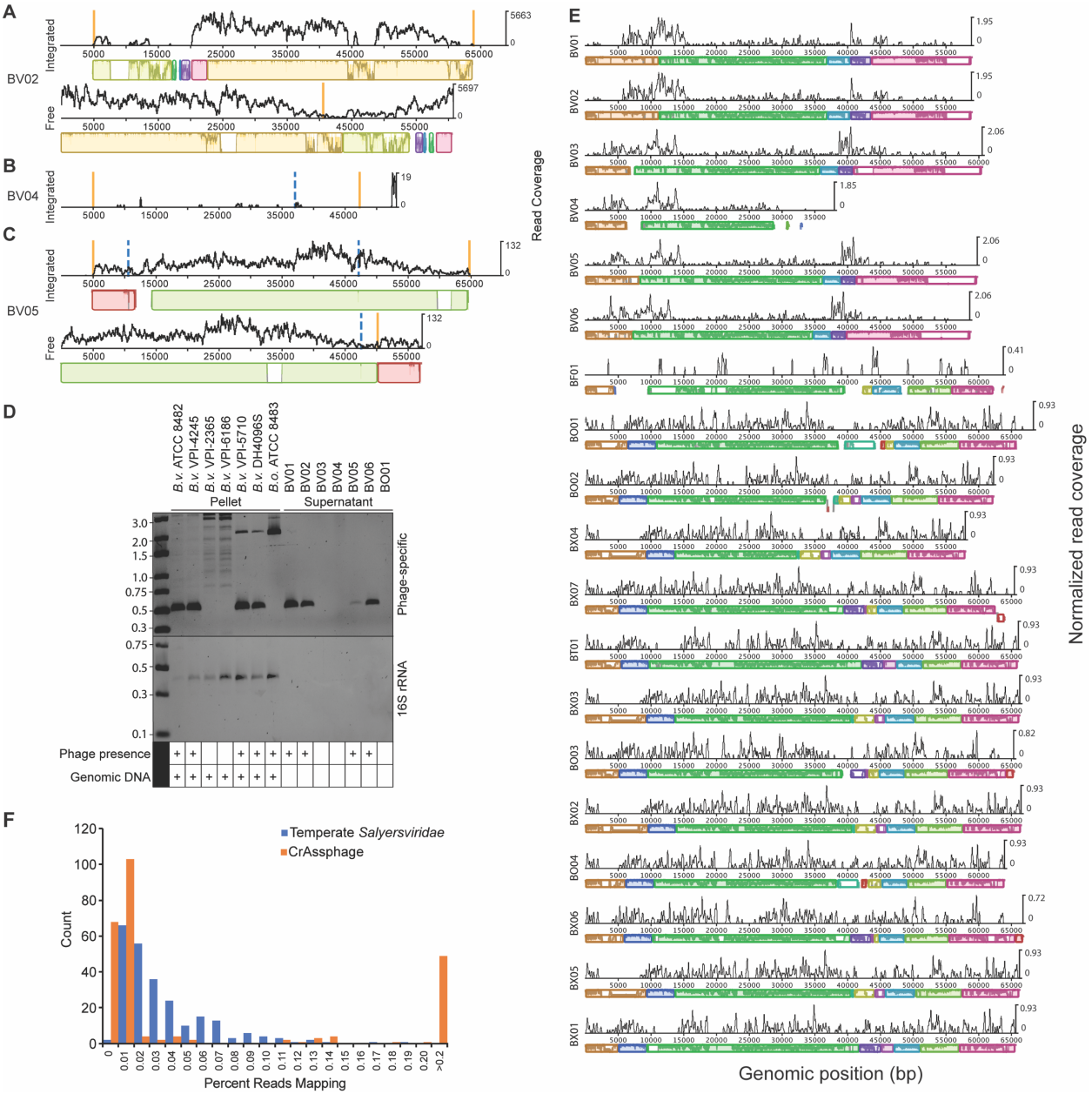

Figure S5. Confirmation of activity of *Salyersviridae* phages *in vitro* and in human-associated samples. Related to Figure 6. DNase-treated culture supernatants for predicted Salyersviruses BV02 (A), BV04 (B), and BV05 (C) were sequenced. Assembly resulted in contigs corresponding to the free form of phages BV02 and BV05; BV04 did not yield any contigs corresponding to the putative prophage region, suggesting it is inactivated. Assembled free phage contigs were aligned to their integrated prophage region with Mauve (A-C). Sequence reads were mapped back to their free and integrated forms and represented as coverage curves (A-C). Vertical orange lines indicate the location of *att* sequences; vertical dashed blue lines indicate the location of contig breaks. (D) PCR amplification with phage-specific primers tests for phage presence in pellet and supernatant fractions for 7 predicted Salyersviruses. Supernatant fractions were treated with DNase, eliminating all contaminating host genomic DNA, as demonstrated by the amplification of a host marker gene (16S rRNA). BV04 is not detectable in supernatant, supporting the conclusion that it is an inactivated prophage. PCR amplicons were visualized by agarose gel electrophoresis alongside GeneRuler Express DNA ladder (16S rRNA); ladder band sizes shown in Kb. (E) Wastewater viromes were collected, and processed in three ways prior to sequencing (see Methods). Resulting reads were trimmed, pooled, and mapped to all *Salyersviridae* genomes and crAssphage. Only *Salyersvirinae* genomes shown in alignment to better demonstrate conservation, constructed with Mauve. Read coverages normalized to total number of reads in the metavirome. The

maximum normalized read coverage for BC01 is 4.1, B40-8 and B124-14 is 1.13, and crAssphage is 7.33. (F) Reads from 246 healthy human gut metagenomes were obtained from the Human Microbiome Project Healthy Human Subjects Study. Reads were mapped to all 20 temperate *Salyersviridae* phages and crAssphage. Percent reads mapping was calculated on a per sample basis as the number of reads mapping to any virus divided by the total number of reads. Histogram shows counts of samples.